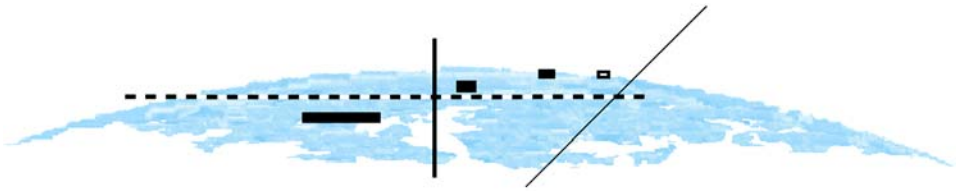

GeoForschungsZentrum Potsdam

STIFTUNG DES ÖFFENTLICHEN RECHTS

Scientific Technical Report

ISSN 1610-0956

Probabilistic Seismic Hazard Assessment for Vanuatu

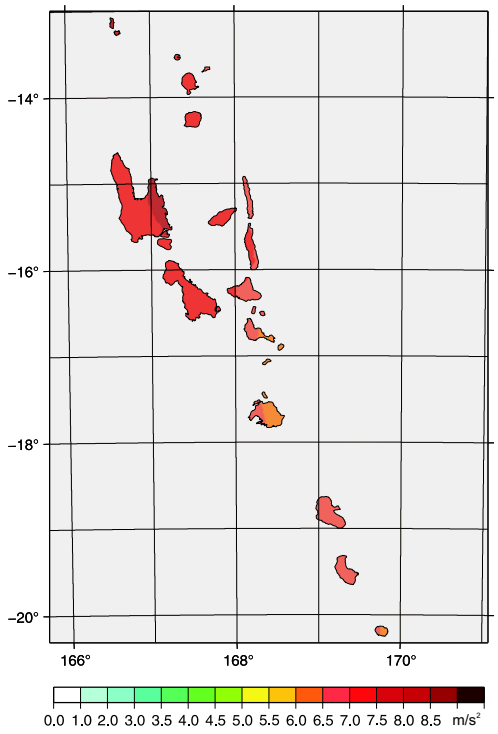

J. Suckale[1], G. Grünthal[1], M. Regnier[2], C. Bosse[1]

[1]GeoForschungsZentrum Potsdam, Telegrafenberg, D-14473 Potsdam,
email: suckale@gfz-potsdam.de
[2]Institut de Recherche pour le Développement, Unité mixte de recherche - Géoscience Azur, 250 rue Albert Einstein, Sophia Antipolis, 06560 Valbonne

Scientific Technical Report STR 05/16

Contents

List of Figures

1. Introduction

The hazardous effects of earthquakes can be divided into three categories: (1) those effects resulting directly from a certain level of ground shaking, (2) those effects on the land surface resulting from faulting or deformations, and (3) those effects triggered or activated by a certain level of ground shaking such as the generation of a tsunami or a landslide. The first category is referred to, when talking about seismic hazard. The other phenomena can be assessed on the basis of this information.

Two approaches are traditionally used in the estimation of seismic hazard - the deterministic and the probabilistic method. The deterministic method attempts to determine a maximum credible intensity of ground-motion at a given site through estimation of a maximum credible earthquake likely to take place in the proximity of that site. This method was applied in an earlier assessment of the seismic hazard in Vanuatu, accomplished by ORSTOM (Office de la recherche scientifique et technique outre-mer), Noumea (Prévot and Chatelain, 1984). However, given the very limited macroseismic database and the few reliable intensity estimates available for Vanuatu, we consider the second, probabilistic approach to be more appropriate. With respect to the geographical setting of the Republic of Vanuatu we refer to Fig. 1.1.

Seismic hazard is defined as the probability that the ground-motion amplitude exceeds a certain threshold at a specific site. The hazard-relevant quantity calculated is the peak ground acceleration (PGA given in m/s^2), a commonly used parameter in earthquake engineering. The methodology applied is based on the generally accepted concept by Cornell (1968) and McGuire (1976).

The purpose of this study is to refine the probabilistic seismic hazard assessment for Vanuatu. The analysis is complicated by inconsistencies of the global and local data for the investigated region and systematic inadequacies of the attenuation relation available. An additional aspect in the field of which more research would be desirable is the de-clustering algorithm for the identification of dependent earthquakes. In order to quantify the inevitable uncertainties associated with our results, we used a Logic Tree approach.

The report is subdivided into seven chapters. Chapter 2 summarises the geology and tectonic setting of the Vanuatu island arc. Prior scientific investigations will be sketched briefly and to the degree to which they are relevant for our further considerations. The consecutive Chapter 3 describes the different data sources used for the calculations. Together, the local earthquake catalogue provided by the

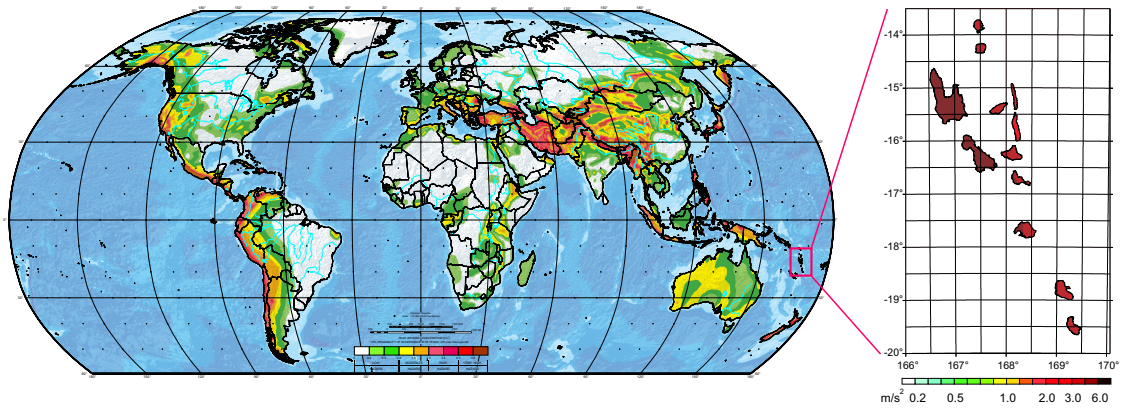

Fig. 1.1: The world map of seismic hazard as compiled in the course of the Global Seismic Hazard Assessment Programme (GSHAP) by Shedlock et al. (2000). The Vanuatu region is framed in red and enlarged. This rough hazard estimate for Vanuatu will be refined in this study (cf. Chapter 7).

IRD (Institut de Recherche pour le Développement) and the global catalogues constitute a comprehensive data base for the region. The homogenisation of different catalogues required the conversion of magnitudes through maximum likelihood regressions. Chapter 4 gives a brief overview over the methodological concept applied. The implementation of the Cornell methodology involves two key steps: The first step is to construct a seismicity model (Chapter 5) including the definition of source zones and seismicity parameters characterising the level and type of activity in the respective zone. The second step is to determine an appropriate attenuation relation for the earthquake-generated ground motion in dependence of magnitude and distance. Chapter 6 compares several attenuation relations from the recent geophysical literature. We argue that the modeling of attenuation is the weakest link in this analysis and the major source of uncertainty. The new seismic hazard maps are presented and discussed in Chapter 7. The map that we consider to be the most relevant is also shown on the inner title page of this report. Our findings indicate that the seismic hazard in Vanuatu has been underestimated by prior assessments such as the Global Seismic Hazard Assessment Programme GSHAP (cf. Fig. 1.1).

Apart from New Zealand (Stirling et al., 2002), Fiji (Jones, 1997), and Australia

(Gaull et al., 1990) few systematic hazard assessments are available for countries in the South West Pacific. Our work aims to help fill this lacuna. We consider our results to be of preliminary nature. Further research in several areas (outlined in Section 7.4.3) would improve the adequacy of our assessment.

This report is the result of a joint cooperation between the GeoForschungsZentrum Potsdam (GFZ), Germany, the Institut de Recherche pour le Développement (IRD), France, and the South Pacific Applied Geoscience Commission (SOPAC), Fiji. SOPAC's long lasting experience and effort to assess natural hazards in the Pacific complemented the scientific investigations pursued and the local seismic data assembled by IRD. The GFZ contributed scientific and technical expertise concerning probabilistic hazard calculations and the financing during the final phase. The initial phase of the project was financed and supported by the Robert Bosch Foundation.

2. Geological and Tectonic Setting

Numerous publications describe the geology and tectonics along the Vanuatu island arc. This chapter briefly summarises those results most relevant for our analysis and gives an overview over the various distinct geological features within the region.

2.1 Geomorphology of the arc

The Vanuatu islands arc lies in the centre of a chain of active islands which mark the present-day boundary between the Australian (Australia-India) plate and the microplate of the North Fiji basin. The islands arc extends about 1 200 km along a NNW-SSE trend between latitudes 10° and 22°S from the Solomon arc in the north to the Matthew-Hunter ridge in the south. Though apparently simple on a large scale, the upper plate is morphologically complex with the most striking structural anomalies occurring in the central part between $14° - 18°$ S. The trench vanishes in this region offshore of Espiritu Santo and northern Malekula and splits the subduction zone into two parts (as shown in Figure 2.1): the northern and the southern segment (Chatelain et al., 1986; Greene et al., 1994). Geomorphologically, the archipelago consists of three major physiographical provinces: trench, arc platform, and backarc.

2.1.1 Trench

The trench is the seafloor expression of an east-dipping subduction zone, locally reaching up to 7 000 m in depth. The subducted plate has an unusually sharp downbent profile and a steep dip (70°) at intermediate depths. The convergence direction is nearly perpendicular to the N 20° W trend of the trench (see Figure 2.1) with a convergence rate varying considerably between 30mm/yr and 124mm/yr (Calmant et al., 2003).

The morphology of the forearc slope varies from a relatively smooth and narrow ($\sim$ 40 km wide) in the north to an irregular, less steep, wide ($\sim$ 80 km wide) feature in the south. In the central part, the forearc slope is quite narrow (only about 20 km wide) and exhibits a distinct westward offset by approximately 35 km.

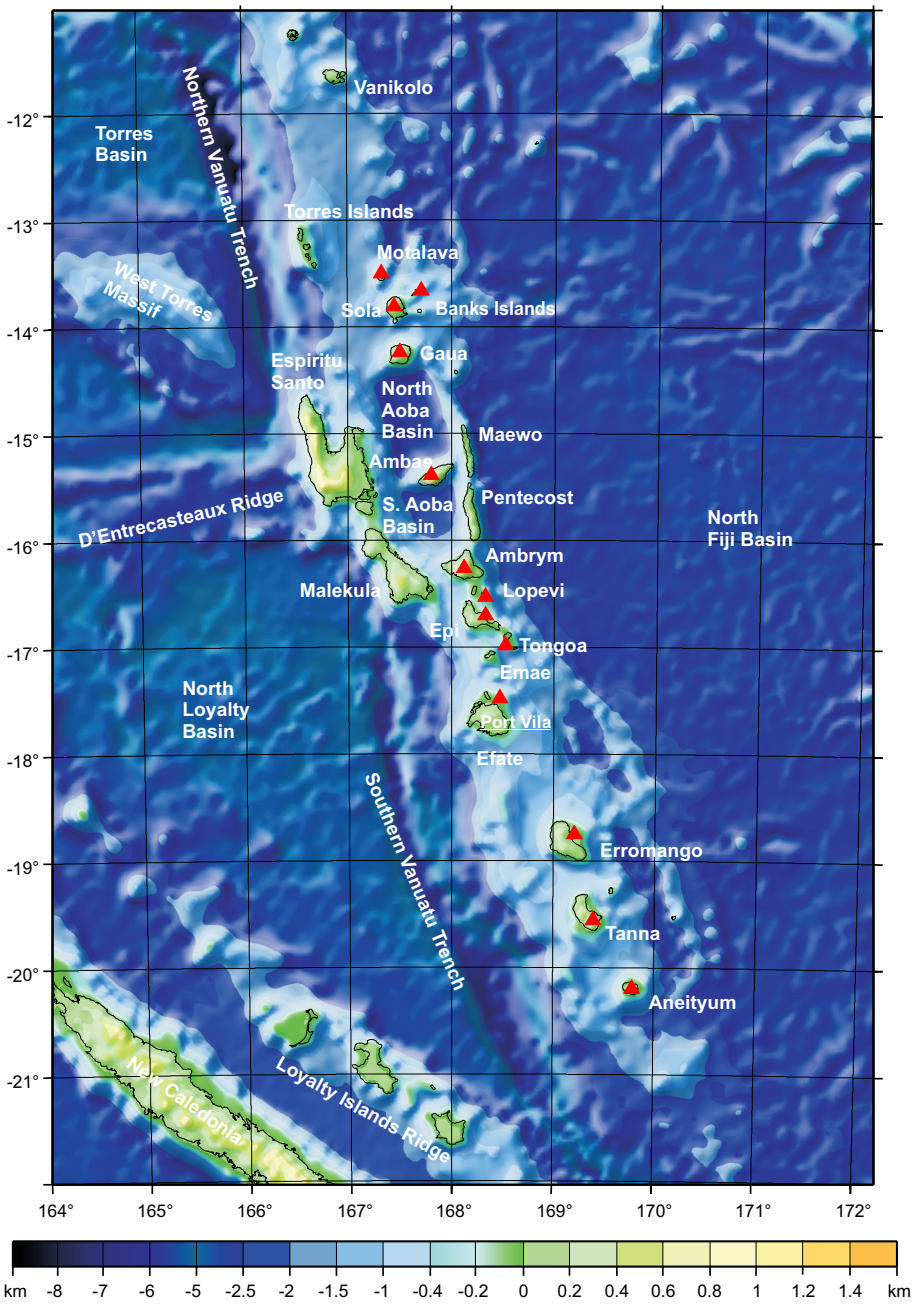

Fig. 2.1: Bathymetric map of the Vanuatu island arc. The colour intervals are irregular in order to display the entire depth range in a satisfactory manner. The major islands and important geological features are named. The most active volcanic regions are indicated by red triangles.

2.1.2 Arc platform

The arc platform has an irregular topography consisting of several basins and ridges. In accordance with the trench, the northern and central parts of the archipelago can be divided into three distinct volcano-tectonic provinces, which are, from oldest to youngest, the western belt, the eastern belt, and the central chain. The western belt (upper Oligocene to middle Miocene) comprises the Torres group of islands, Espiritu Santo and Malekula; the eastern belt (Mio-Pliocene) consists of Maewo and Pentecost. The central chain (Banks islands, Ambae, Ambrym, Lopevi, Epi, Tongoa, Efate, Erromango, Tanna and Aneityum) is the presently active or recently quiescent volcanic arc that is as old as 5.8 Ma in the southern part, but no older than Pleistocene in the central part (Colley and Ash, 1971). Its location varies along the arc lying generally 150 km east of the trench in the north and the south, but only $\sim$ 100 km east of the trace of the trench in the central part of the arc (Greene et al., 1994).

Within the platform of the central Vanuatu island arc and bounded on the east by the backarc zone is an intra-arc sedimentary basin. This basin is divided into two separate and distinct physiographic basins, the North Aoba basin and South Aoba basin with water depth of $2\,000 - 3\,000$ m. No intra-arc basin exists south of Ambrym and north of Gaua.

2.1.3 Backarc

The backarc is part of the North Fiji basin. It is itself split into platelets by numerous spreading axes and transform faults (Calmant et al., 2003) and is characterised by irregular seafloor with water depths of $2\,000 - 3\,000$ m. In the central part of the Vanuatu island arc no backarc-like troughs exist that are similar to those present in the north and south (Charvis and Pelletier, 1989).

2.2 Tectonic evolution

The Vanuatu archipelago is a complex tectonic unit, which results from an interplay between the currently active subduction, the collision with several major submarine ridges and basins, and the spreading of the North Fiji basin. It is thought to have originated in the Eocene as a segment of the now extinct Vitiaz trench, nowadays a fossil boundary to the north of the Fiji basin (see Figure 2.2). During the middle Miocene, the polarity of the arc reversed, probably as a result of the collision of the Ontong Java plateau with the Solomon Islands further northwest along this arc system (Greene et al., 1994). Opening of the North Fiji back-arc basin caused the east-facing island arc to rift from the extinct west-facing Vitiaz trench (Meffre and Crawford, 2001).

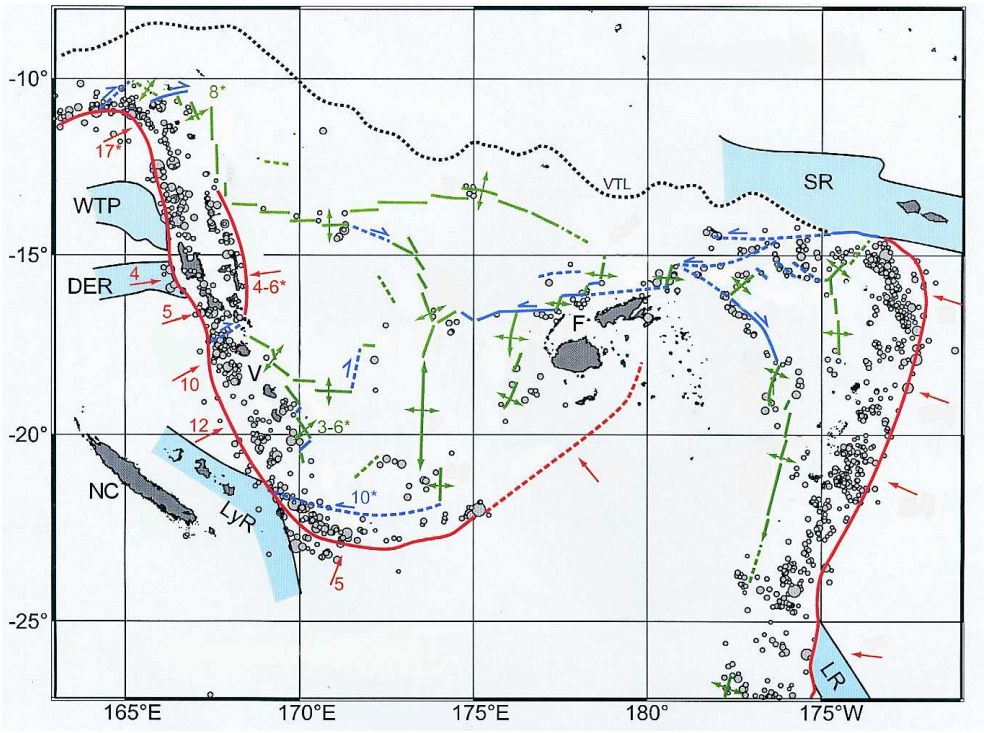

Fig. 2.2: Simplified tectonic map of the Tonga-New Hebrides region according to Pelletier et al. (1998). The displayed earthquakes occurred during the years 1977 – 1996 and were localised by the US Geological Survey USGS/NEIC. The two criteria for the selection of events was that (1) their focal depth had to be below 50 km and (2) that a focal mechanism solution had to be available. The radius indicates the magnitude of the respective event. The other features are meant to clarify the tectonic constellation within the region: Lines or segments show known active plate boundaries, while dashed lines indicate inferred boundaries. Letters refer to Vanuatu (V) and to the neighbouring Island States Fiji (F), and New Caledonia (NC). The dotted black line marks the fossil lineament of the now extinct Vitiaz trench (VTL). The lighter blue regions outline the submarine ridges in the region. These are: the West Torres plateau (WTP), the D'Entrecasteaux ridge (DER), the Loyalty Islands ridge (LyR), the Samoan ridges (SR) and the Louisville ridge (LR). The arrows show the convergence direction and rate in cm/yr as determined by Pelletier et al. (1998). The colours indicate the type of convergence: subduction movements are marked in red, spreading zones in green, and transformation zones in dark blue.

2.2.1 Submarine ridges

The structure of the Vanuatu island arc has been significantly modified by the collision with three major submarine ridges, which are from north to south the West Torres plateau, the D'Entrecasteaux ridge and the Loyalty Island ridge. Collision is assumed to have caused uplift of the trench and forearc (up to 6 000 m), subsidence around the arc volcanic edifices (up to 2 500 m), forming a large intra-arc basin, and uplift of the arc-backarc transition (up to 2 000 m) (Meffre and Crawford, 2001).

The West Torres massif is a submarine flat-topped plateau about 35 000 km^2 in size, which is rising up to 4 000 m above the surrounding sea floor. Little is known about its age and tectonic origin. Analogous to the D'Entrecasteaux ridge it is thought to be colliding with the central section of Vanuatu (Taylor et al., 1995). According to Meffre and Crawford (2001), the shape and topography of the massif and the shallow trench seem to indicate that at least 60 km of the West Torres massif has been subducted beneath the island arc, significantly altering its morphology.

The D'Entrecasteaux ridge is a curved aseismic feature on the subducting Australian plate, that extends from New Caledonia to the central Vanuatu arc. Bathymetric data indicate that it is a twin-spined ridge (cf. Figure 2.1), comprising a high relief ($2 - 4$ km) northern ridge and a southern chain. The east trending D'Entrecasteaux zone is slightly oblique (14° to the estimated direction of plate convergence) and creeps slowly northwards at an average speed of about 2.5 cm/yr, thus causing a continual structural deformation of the accretionary complex (Collot et al., 1985; Collot and Fisher, 1991; Collot et al., 1991a).

Various interpretations have been proposed for the tectonic setting of the D'Entrecasteaux ridge. Collot and Fisher (1991) concluded that it may be a fossil plate boundary, because seismic refraction velocities (Pontoise and Tiffin, 1986), basement morphology, and sediment characteristics (Burne et al., 1988) suggest that the crustal material of the North Loyalty and the Torres basin had different origins. The Loyalty islands ridge is on the border of our region of interest and will not be discussed further.

2.2.2 Convergence rates

Pelletier et al. (1998) derived an up-dated tectonic map for the North Fiji basin region displayed in Figure 2.2. They argue that instead of a diffuse and shear dominated seismicity model as previously proposed by Hamburger and Isacks (1988), a deformation distributed on numerous spreading ridges is more adequate.

The region is characterised by a large variation in both consumption rate along the arcs and opening rate along the back-arc basins spreading centres. The highest convergence (124 mm/yr) is found at Tanna while the lowest (28 mm/yr) is found on Malekula (Calmant et al., 2003). Generally, rapid subduction correlates with fast

backarc-opening. Pelletier et al. (1998) observe anomalous features in the collision areas with the submarine ridges: the convergence slows down and arc-transverse strike-slip faulting is found as well as slow backarc-spreading.

2.2.3 Uplift of the trench and the arc platform in central Vanuatu

Apart from the low convergence velocity, the central area of the Vanuatu island arc as defined in Section 2.1.1 is characterised by several other unusual features, the most prominent being the very shallow trench and the large islands in the forearc. These islands are located 30 km from the zone of subduction - in a position that would normally correlate with the middle of the trench arc slope in most intraoceanic island arcs.

These anomalies have been related by several authors to the effects of the subduction of the D'Entrecasteaux zone (Maillet et al., 1983; Pascal, 1974; Choudhury et al., 1975). However, Collot et al. (1985) pointed out that the subduction of a ridge would theoretically be expected to cause both a shift of the plate boundary towards the arc and a shallowing of the trench (cf. (Vogt et al., 1976)). These effects have been attested for the subduction of the Louisville ridge beneath the Tonga arc (Dupont, 1979, 1982), but are not seen in central Vanuatu, where the plate boundary is displaced away from the arc, and no trench is developed (cf. Figure 2.2). Therefore, Collot et al. (1985) and Daniel and Katz (1981) concluded that the presence of rigid, old (Miocene) crustal blocks in the forearc is a second major factor influencing the deformation of the plate contact zone.

Meffre and Crawford (2001) pursued a global study of selected island arcs and argue that the $3\,000 - 4\,500$ m uplift of the trench in Vanuatu is almost entirely due to collision. They suggest that only a small amount of variation (approximately 1 000 m) in the trench depth could be accounted for by differences in the age of oceanic basins, which are being subducted beneath the arc and in the geometry of the plate boundary. Furthermore, they presume that previous studies (Chung and Kanamori, 1978; Collot et al., 1985; Greene et al., 1994; Geist et al., 1993; Taylor et al., 1995) largely underestimated the deformation of the trench caused by the collision of the West Torres massif and suggest that it is approximately equal in size compared to the uplift caused by the d'Entrecasteaux ridge.

From a geophysical point of view one would expect that the very large rates of uplift observed in the forearc (Taylor et al., 1990, 1995) would be associated with extensive faulting or folding at the surface of Espiritu Santo or Malekula. However, experimental data does not clearly confirm this. The results from the Ocean Drilling Project (Greene et al., 1994) indicate that a large number of straight strike-slip faults related to the recent collision cut across the entire arc. However, Meffre and Crawford (2001) could not confirm this result through analysis of aeromagnetic or surface information. They suggest that the forearc is divided into $50 - 100$ km long

blocks, with would be in accordance with Taylor et al. (1990), who found differences in the rates and pattern of uplift between different areas in forearc.

Uplift in the backarc is not as large as in the forearc, but faulting and folding are more intense, particularly at shallow levels within the crust. An example of this deformation is the fold and thrust faults in the youngest sediments on the eastern margins of the North Aoba basin (Pelletier et al., 1994).

2.2.4 Subsidence of the intra-arc basins

In the Vanuatu island arc uplift in the forearc is accompanied by subsidence in the intra-arc basins. The amount of subsidence is approximately half the amount of uplift in the forearc (Meffre and Crawford, 2001).

In the course of the Ocean Drilling Program, Greene et al. (1994) collected data from sites within the North Aoba basin. The data suggests that the deepening occurred between 1.8 and 1.5 Ma. This unconformity has been interpreted as the beginning of the collision in the Espiritu Santo area. Shallow equivalents of these intra-arc basins were already present prior to collision as the basin contains a thick sequence of Miocene to Pliocene sediments (Fisher et al., 1994). In the transition zone between collisional and non-collisional sections of the arc, subsidence occurs in the forearc and uplift occurs around the arc volcanoes.

2.2.5 Crustal shortening

A zone of crustal shortening extends along the eastern margin of central Vanuatu from 13°30'S to 16°30'S in front of the subducting d'Entrecasteaux and West Torres ridges. Contrary to the rest of the island arc, seismic activity is higher along the eastern margin than along the western margin of this area. Pelletier et al. (1998) proposed a present-day crustal shortening rate of 5.5 cm/yr.

GPS measurements (Pelletier et al., 1998) indicate that the central Vanuatu arc slowly converges relative to the Australian plate and moves eastward relative to the southern part of the arc along a dextral strike-slip zone. Furthermore, bathymetry, seismicity and GPS data indicate that a transverse-arc shear zone extends from the trench west of Efate island to south of Epi island at the junction area between the southern Vanuatu backarc troughs and the central backarc compressional zone.

3. Seismicity Data

Three different data sources have been merged to constitute the seismicity catalogue for Vanuatu: the United States Geological Survey / National Earthquake Information Centre (USGS/NEIC) catalogue, the Engdahl catalogue (Engdahl et al., 1998) and a local catalogue provided by the Institut de recherche pour le développement (IRD). The usage of different data sources is motivated by their mutual incompleteness. The area of investigation has been specified as: $11°\mathrm{S} - 22°\mathrm{S}$ and $164°\mathrm{E} - 172°\mathrm{E}$ (cf. Figure 2.1). The seismic activity outside these margins can be considered as negligible. The final catalogue has been constituted according to the following priorities: All events as given in the USGS/NEIC catalogue are included and complemented by those events from the Engdahl catalogue that are not yet listed. Additionally, those local recordings that have not been registered globally are taken into consideration.

3.1 Global catalogues

After combining the two global catalogues by USGS/NEIC and Engdahl et al. (1998) our database contains a total of 7 519 events for the time period from $1964 - 2003$ within the area specified above. The epicentres of these events are displayed in Figure 3.1. At first sight the seismicity seems to be rather homogenously distributed, but a more detailed analysis of the focal depth distribution uncovers several anomalous features.

3.1.1 USGS/NEIC

The United States' Geological Survey USGS/NEIC monitors a global catalogues from 1973 until today. For the Vanuatu region it contains a total of 7 708 events until December 2003. In order to consider an event in our calculations the following minimal information must be given: date, origin time, localisation, focal depth, and a magnitude of specified type - those events with 'unknown magnitude type' are not included. This restriction leaves 6 735 usable events.

In addition to this catalogue, USGS/NEIC and the National Geophysical Data Center of the National Oceanic and Atmospheric Administration (NOAA) provide a list of significant historical worldwide earthquakes. Due to the approximative nature of magnitude and localisation estimates for pre-instrumental events those are not

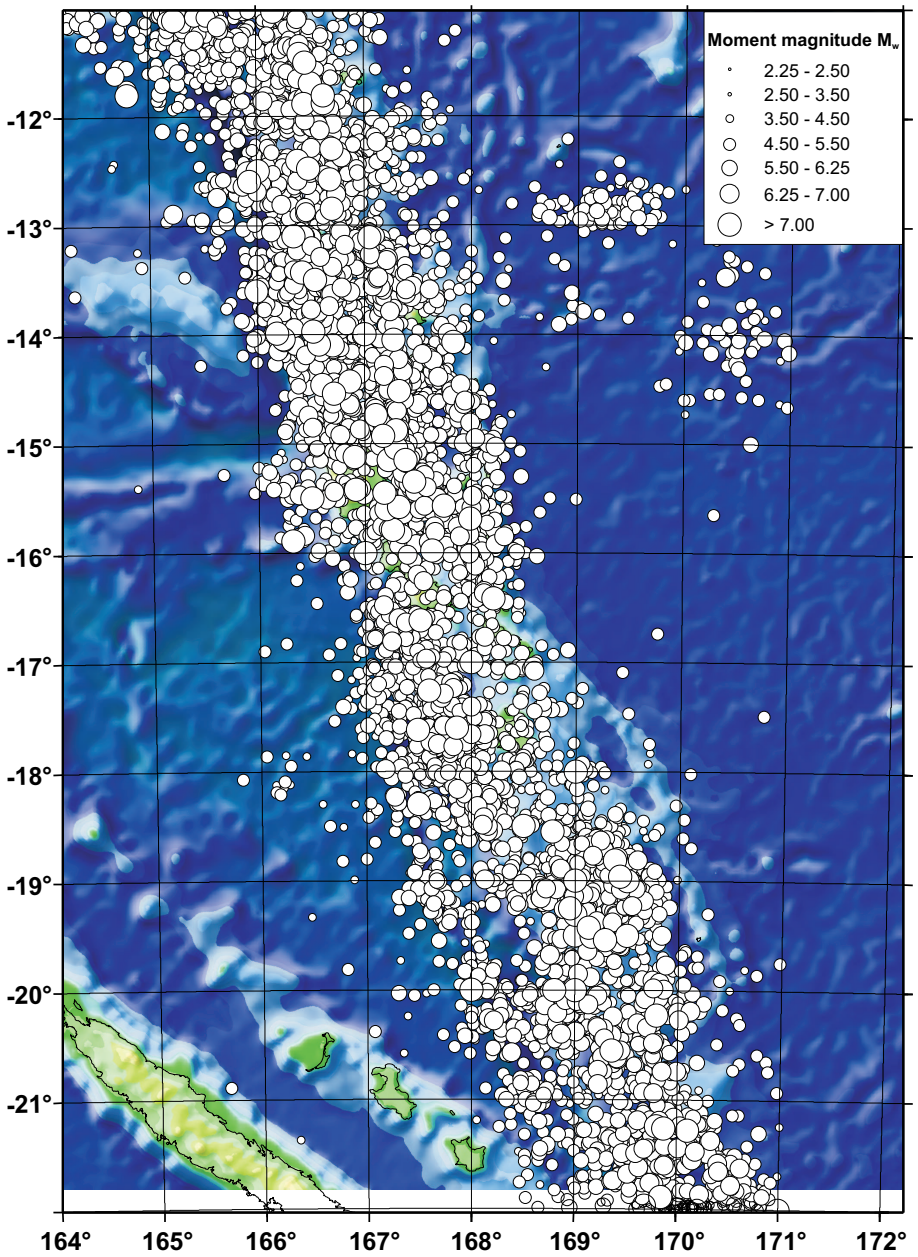

Fig. 3.1: Map showing the epicentres of all globally measured events taken from Engdahl et al. (1998) and the USGS/NEIC catalogue. The earthquakes are grouped into moment magnitude classes, with the shown radius indicating the magnitude of the respective event. The legend in the upper corner of the figure summarises the correspondence of radius and moment magnitude M_w.

used for the calculations, though. The USGS/NEIC catalogue is the most comprehensive, but the information given for each earthquake is comparatively less precise. The depth inaccuracy is particularly problematic. Most events have been assigned a default depth instead of a properly calculated value.

3.1.2 Engdahl catalogue

The catalogue by Engdahl et al. (1998) lists 3 257 events for the time period $1964 - 2002$. Out of these, 3 224 are theoretically usable. However, we expect that the great majority of events listed by Engdahl et al. (1998) is also contained in the USGS/NEIC-catalogue. In order to avoid double-counting, recordings that refer to earthquakes already listed have to be identified and excluded. We consider two events to be identical, if they describe earthquakes that lie within a time-frame of 20 s and a space-frame of 50 km of each other. The estimated magnitude for thus identified identical events usually corresponded well, albeit some exceptions differing by close to $+/-1$ magnitude unit. Where duplets exist, the NEIC solution is preferred for reasons of completeness and consistency (almost three times as many annual events given by NEIC compared to Engdahl et al., 1998). After eliminating the duplets, 784 Engdahl et al. (1998) entries remain in our final catalogue, most of which in the time period 1964 - 1972.

3.2 Local catalogues

A network of 19 telemetered seismograph stations was operated from $1978 - 1990$ as a joint project between ORSTOM and Cornell University. The operation of this network was reassumed in 1994 after technical adjustments and continued until 2002. For both time spans, in the following referred to as first and second measurement period, the localisations and magnitudes were provided by the Institut de Recherche pour le Développement (IRD). Moment magnitude M_w estimates are assigned to local events, originally based on coda magnitude M_c or on local magnitude M_L respectively according to regressions particularly developed for this purpose (cf. Section 3.3).

3.2.1 First measurement period

The local catalogue lists 26 245 events, given in coda magnitude M_C for the years $1978 - 1990$. The epicentres are plotted in Figure 3.2 (map on the left). Two features in this figure merit further discussion: First, it is obvious that the coverage of the local network is considerably smaller than that of the global catalogues. This problem persists for the depth distribution of events. Second, many of the large events are missing. This incompleteness for higher magnitudes results from the saturation of

the seismographs and the radio transmitters used. For the purposes of this study, this incompleteness of the local catalogue is a major obstacle as these events are obviously the most relevant for hazard assessments.

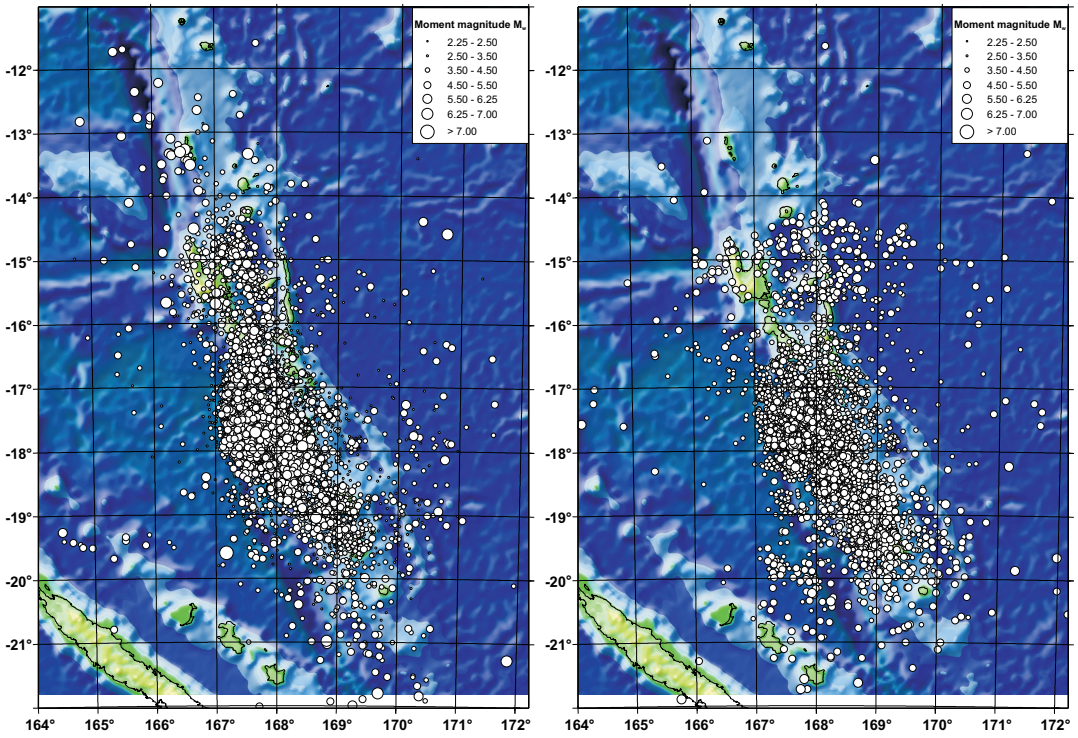

Fig. 3.2: These two maps show the epicentres of the events as registered by the local network sustained by Cornell University in cooperation with IRD. The map on the left shows the first measurement period from 1978 to 1991, the map on the right refers to the data obtained during the second measurement period from 1994 to 2002. The magnitude classes correspond to those used in the epicentre map for the global catalogue 3.1. Apart from the limited coverage of the local data, it is obvious, that the local catalogue is incomplete for strong magnitudes.

Evidently, the local recordings contain many events also listed in the global catalogues. As already stated above earthquakes occurring within 20 s and 50 km of each other are considered identical. When choosing whether to keep the local or the global data given for the same earthquake, priority was given to the global catalogues due to the saturation problem. Thus, out of 19 208 theoretically usable data sets 18 409 were kept for the final catalogue. The inclusion of these events requires the conversion of local or coda magnitude to moment magnitude (see Section 3.3 and Appendix B).

3.2.2 Second measurement period

Operation of the local network was reassumed in 1994. The localisation of the earthquakes is based on fewer stations than during the first measurement period. And contrary to before, the local magnitude M_L is used instead of coda magnitude M_C to characterise the size of earthquakes. In 1997 technical adjustments were undertaken - data from this year may be partly incomplete. From the second measurement period 16 529 events are contained in the final catalogue.

3.3 Magnitude conversion

The final catalogue for the Vanuatu region contains five different types of magnitudes: moment magnitude M_w, body wave magnitude m_b, surface wave magnitude M_S, coda magnitude M_C and local magnitude M_L. In order to convert them to M_w we derived regressions based on the Maximum likelihood approach for each of these cases. The regressions were carried out assuming that the error of the M_w value and the respective other magnitude type is equal. For the derivation of the following equations see Appendix B.

$$M_w = 1.2690 M_S - 1.0436 \quad \text{for the USGS/NEIC catalogue} \tag{3.1}$$
$$M_w = 1.2765 M_S - 1.0825 \quad \text{for the Engdahl catalogue} \tag{3.2}$$
$$M_w = 0.7813 m_b + 1.5175 \quad \text{for the USGS/NEIC catalogue} \tag{3.3}$$
$$M_w = 0.7601 m_b + 1.6562 \quad \text{for the Engdahl catalogue} \tag{3.4}$$
$$M_w = 1.0583 M_C + 0.1765 \tag{3.5}$$
$$M_w = 0.6960 M_L + 1.7738 \tag{3.6}$$

Both global catalogues comprehend multiple events for which mutual estimates of M_w, M_S, and m_b are given. In that case the original M_w value is of course kept. If values for both m_b and M_S are available, M_w is preferably derived from m_b.

3.4 Completeness

To check the magnitude dependent effectual completeness of the catalogue, the cumulative number of earthquakes per magnitude class is plotted in Figure 3.3. This method (used by Grünthal et al. since the 1980s) is only applicable to the global data, because the registration gap of the local network is not accounted for in this kind of diagram. A magnitude class is complete from the year from which onwards a roughly constant slope can be assigned to the cumulative number of earthquakes in the respective magnitude range. Only the effectual complete time and magnitude intervals will be calculated with.

Moment magnitude class	Complete since
4.3 – 4.7	1995
4.8 – 5.2	1988
5.3 – 5.7	1964
5.8 – 6.2	1964
6.3 – 6.7	1964
6.8 – 7.2	1964
7.3 – 7.7	1964
7.8 – 8.2	1964

The strongest earthquake in the study area since 1964 (with an estimated moment magnitude of $M_w = 7.8$) is found in the Engdahl catalogue for July 17th, 1980. However, several other events of comparative size have been recorded in Vanuatu. The list of historical earthquakes in the region even contains events up to $M_w = 8.1$. However, the considerable uncertainty associated with the exact magnitude estimate and localisation of these impedes their inclusion in our calculations.

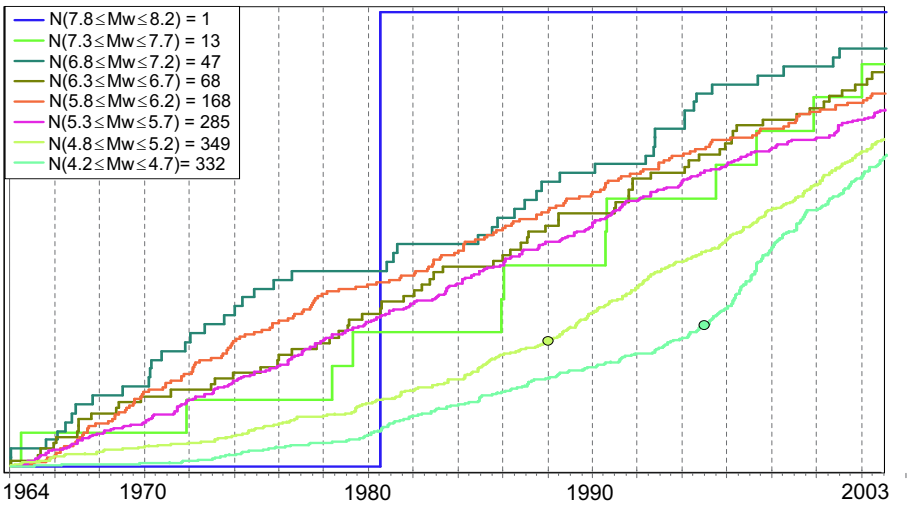

Fig. 3.3: The figure shows the cumulative number of earthquakes in the respective magnitude class for the global catalogue. Each of the differently coloured standardised graphs represents the frequency of occurrence in one magnitude class. The total number is given in the upper left corner. A magnitude class is considered complete (in the sense that all earthquakes of that size are contained in the catalogue) if the graph is fairly linear. For the two smallest magnitude classes, the year from which on the class is considered complete is designated by a dot on the respective graph. The others are complete from 1964 on. A table of completeness by magnitude class is given in the text.

4. Methodology

The basic assumption of hazard assessments is that earthquake activity will recur where it was observed in the past or where it can be expected in future. The latter can include areas which are tectonically prone to earthquakes which were not recorded in the historical past. The occurrences of earthquakes are considered probabilistically. Cornell (1968) suggested to randomise the observed seismicity in both time and space. This is achieved by modeling the seismicity in zones with uniform spatial and temporal probability of earthquakes occurrence. These so-called 'source zones' are chosen on the basis of structural geological and neotectonic data and the seismicity registered or historically observed.

4.1 Probabilistic seismic hazard assessment (PSHA)

The seismic hazard $H(A)$ is defined as the annual rate of earthquakes that produce a ground-motion amplitude a exceeding the expectation A at a specific site. The random variable a may generally represent an arbitrary hazard-relevant quantity describing the ground shaking. In this study it is the peak ground acceleration, abbreviated by PGA.

Based on Cornell (1968) and McGuire (1976) the overall hazard is composed of the respective contribution $H_i(A)$ from each source zone i out of the set of zones I. Thus, the seismic hazard is evaluated for each zone separately and then summed over. According to the total-probability theorem it is given by

$$H(A) = \sum_{i \in I} H_i(A) = \sum_{i \in I} \nu_i \int_{m_{min}}^{m_{max}} \int_{r_{min}}^{r_{max}} P(a > A|m, r) f_{R_i|M_i}(r|m) f_{M_i} \, \mathrm{dr} \, \mathrm{dm} \qquad (4.1)$$

where ν_i is the annual rate of earthquakes with a magnitude higher than a yet to be specified threshold value M_{min_i} in the zone i. f_{M_i} and $f_{R_i|M_i}(r|m)$ are the probability density functions on magnitude and distance and $P(a > A|m, r)$ is the probability that the expectation A of the ground acceleration is exceeded under the condition that an earthquake of magnitude m occurred at distance r. A hazard curve $H(A)$ is obtained by performing the above calculation for multiple A values. Throughout the analysis, we assume that the number of earthquakes happening during a time

interval Δt can be adequately approximated by a Poisson distribution:

$$P(K = k, \Delta t) = \frac{\lambda^k}{k!} \exp(-\lambda) \tag{4.2}$$

with $P(K = k)$ being the probability that k events occur during Δt and λ the expectation of the number of earthquakes in Δt.

Assuming a Poisson distribution implies that the events are statistically independent, which is only true if the fore- and aftershocks are separated out from the seismicity catalogue. Therefore, the catalogue has to be de-clustered, thus reducing it to a set of uncorrelated earthquakes considered as main shocks. The identification of dependent earthquakes proved to be problematic for Vanuatu. The adequacy of the de-clustering algorithm is tested in Section 4.1.2.

Seismic source zones are assumed to have homogenous seismicity, in the sense that the earthquake locations and magnitudes are uniformly distributed in space. This assumption is required to ensure the existence of a unique probability density function, which is characteristic for the specific zone. It is based on the past activity in the zone according to the catalogue used. The probability density function on magnitude is defined as the derivative of the yearly occurrence rate N_j by magnitude dm for all zones $i \in I$:

$$\begin{aligned} \frac{N_i(m)}{\mathrm{d}m} &= \nu_j \frac{df_{M,i}(m)}{\mathrm{d}m} \\ &= \nu_i \begin{cases} 0 & \text{for} \quad m \in (-\infty, m_{min}) \\ \frac{\exp(-\beta_{ji} m)}{C_i} & \text{for} \quad m \in [m_{min}, m_{max}) \\ 0 & \text{for} \quad m \in [m_{max}, \infty) \end{cases} \\ \text{where} \quad C_i &= \frac{\exp(-\beta_j m_{min}) - \exp(-\beta_j m_{max})}{\beta_j} \end{aligned} \tag{4.3}$$

The respective zones are characterised by the parameters ν_i (the frequency of earthquakes with $M \geq M_{min_i}$) and β_i (the spatial distribution of earthquakes with $M \geq M_{min_i}$).

4.1.1 Identification of dependent earthquakes

In Vanuatu clustering is mainly limited to shallow depths above 60 km. A similar phenomenon has been observed in other subduction zones by Wyss and Toya (2000). We performed a χ^2-test to evaluate how well the deep events (focal depth below 60 km) can be fitted into a Poisson distribution and obtained satisfactory results (cf. the following Section 4.1.2). It is therefore justified to assume that the deep events are already Poisson distributed, even without applying any de-clustering technique.

The shallow depths range has to be treated differently, since it is characterised by strong clustering (cf. Figure 5.2 for the depth profiles).

The algorithm used to determine the dependent earthquakes is based on Musson (1999). Initially, all events are assumed to be mainshocks and are arranged according to size. In this order, a magnitude-dependent time and space frame is assigned to the mainshocks and all events comprised in it are considered to be dependent. For continental Europe, an adequate size of the time and the space window has been determined by Grünthal (1985) in combination with Gardner and Knopoff's (1974) approach. However, these windows cannot be adopted for a subduction region as active as Vanuatu, since far too many events would be identified as dependent. We therefore reduced the window size considerably. The rationale for choosing a window size is the following: (1) The set of mainshocks has to be Poisson distributed. (2) We expect that $40 - 50\%$ of the events in the seismicity catalogues are mainshocks. This percentage share refers to prior clustering studies such as the one pursued by Reasenberg (1985) for California. In this thorough analysis of background seismicity, the author finds that 48% of all registered events are clusters.

Our calculations show that by reducing the window size derived by Grünthal (1985) to half, we obtain a reasonable number of Poisson-distributed mainshocks. Note that the set of mainshocks remains Poisson distributed if more events are separated out randomly by using larger windows. Thus, the window should be set to the minimal size that yields a Poisson distributed catalogue. This is fulfilled for the above choice.

The results of the de-clustering algorithm for shallow depths above 60 km are given in the following table. Since the clusters overlap, we therefore only list the total number of dependent events and do not differentiate these further.

Tab.: Number of mainshocks and dependent events in the shallow part in the used global catalogues:

Catalogue	**Total**	**Shallow events h < 60 km**	**Number of mainshocks**	**Number of dependent events**
USGS/NEIC	6 735	4 188	1 764	2 424
Engdahl	784	401	189	212
Total	7 519	4 589	1 935	2 636

In the case of Vanuatu the de-clustering algorithm yields approximately 42% main events. The described procedure is without doubt a rough approach and a more subtle analysis of clustering in Vanuatu would definitely be desirable. However, for the purpose it serves in this study, namely to identify a Poisson-distributed set of mainshocks, it is sufficient.

4.1.2 χ^2-tests

We performed several χ^2-tests to verify that the mainshocks in our catalogue are temporally Poisson distributed. We tested two null hypothesis: First, globally registered events below 60 km of focal depth are temporally Poisson distributed (no de-clustering is used). Second, events for shallow depths (above 60 km of focal depth) are temporally Poisson distributed after our de-clustering algorithm is applied. For all tests, we set the minimum magnitude of investigated events to $M_w = 5.3$, because the completeness of the catalogues is required for the test (cf. Section 3.4).

Two exemplary χ^2-tests are shown in Figure 4.1. Each test refers to a specific time interval, which determines the number of classes used for calculating the distribution of the test variable χ^2. In both cases, the null hypothesis that the data follows a Poisson distribution could not be rejected at the 0.1% significance level. Although a certain ambiguity in the choice of time intervals is unavoidable, we conclude that the catalogue contains a set of temporally Poisson distributed mainshocks.

4.1.3 Probability of exceedance

Two concepts are often used to quantify seismic hazard: the mean return period $T := \frac{1}{\lambda}$ of major events and the probability to exceed a certain level of ground motion. For Poisson distributions the probability that at least one event will occur during Δt is

$$P(K \geq 1) = 1 - P(K = 0) = 1 - \exp(-\frac{\Delta t}{T}) \,. \tag{4.4}$$

Thus, we get the following relationship between the probability of exceedance $P(K \geq 1)$ during Δt and the mean occurrence period T (or the frequency ν):

$$T = \frac{1}{\nu} = -\frac{\Delta t}{\ln(1 - P(K \geq 1))} \tag{4.5}$$

From an engineering point of view it has become common practice to consider the acceleration that has a probability $P(K \geq 1) = 0.1$ of being exceeded during 50 years for the earthquake resistant design of structures on the basis of building codes. The corresponding mean return period is 475 years. 0.051ex

4.2 Logic tree approach

In the field of seismic hazard analysis it is essential to differentiate between aleatoric and epistemic uncertainty. Aleatory variability stands for the scatter associated with empirical relationships. The most essential aleatory variability in seismic hazard analysis is associated with ground-motion attenuation relations, which is directly

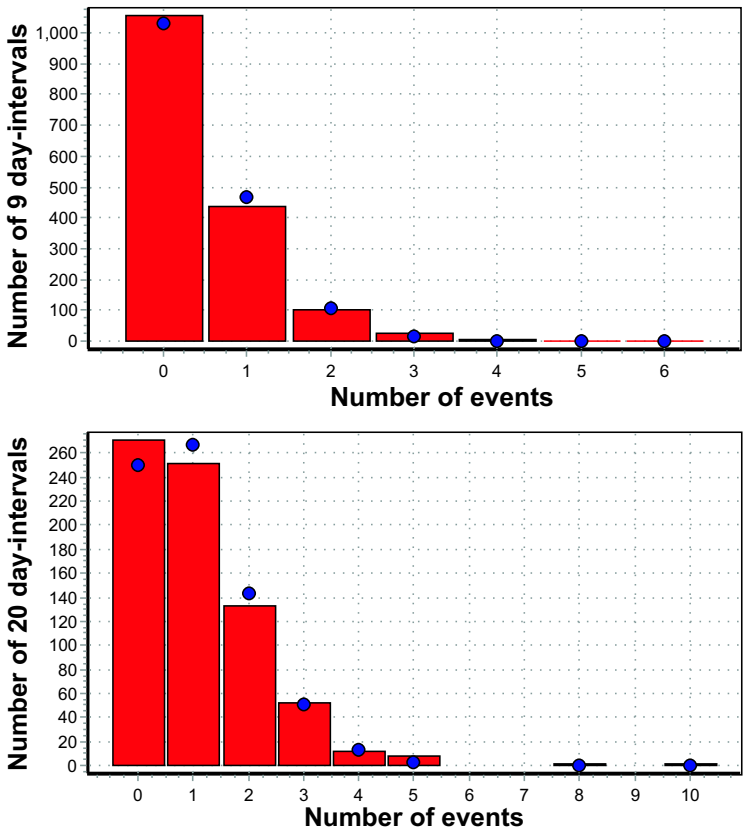

Fig. 4.1: The figures show two exemplary χ^2-test to verify that the mainshocks in our catalogue are temporally Poisson distributed. Both diagrams refer to a specific time interval (9 and 20 days, respectively). The number of time intervals that contain the respective number of events is plotted over the number of events. The red columns represent the actual data and the blue dots the theoretical distribution of the test variable χ^2. The figure on the left shows the χ^2-test for all events below 60 km (730 events) and time intervals of 9 days (yielding 1458 intervals). The figure on the right shows an equivalent χ^2-test for the de-clustered catalogue in shallow depths above 60 km. We used 779 events and time intervals of 20 days (729 intervals altogether). In both cases, the null hypothesis that the data follows a Poisson distribution could not be rejected at the 0.1% significance level.

integrated in the standard practice of PSHA. Epistemic uncertainty reflects the incomplete knowledge of, say, model assumptions like the characteristics of seismic source zones or the maximum magnitudes. These epistemic uncertainties are incorporated into the PSHA through the use of logic trees as done in Figure 4.2. Therein,

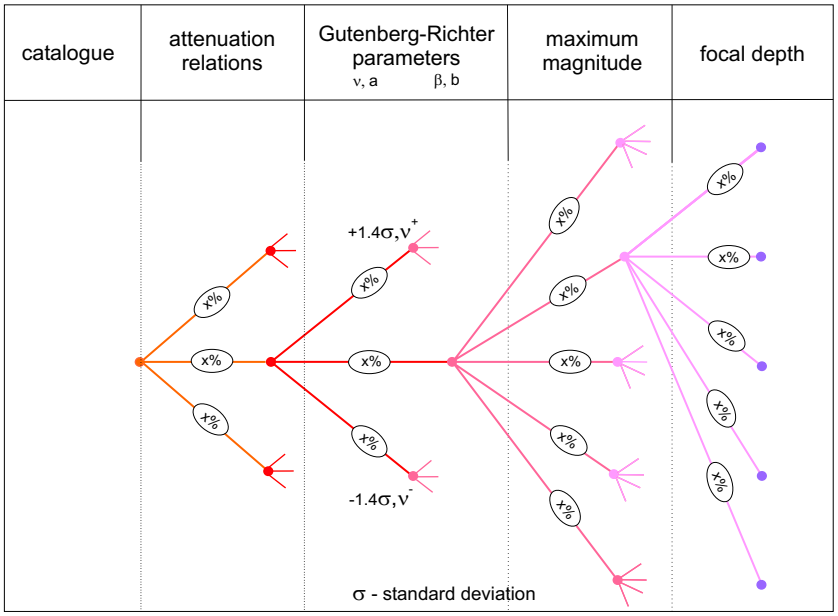

Fig. 4.2: The figure shows a schematic logic tree structure. It is subdivided into core categories crucial for the probabilistic analysis. These are: the catalogue, the attenuation relations, the Gutenberg-Richter parameters, the maximum magnitude and the focal depths.

each level of the tree represents one source of uncertainty; each terminal node represents one "state of nature". Corresponding to each terminal node there is a hazard curve with an assigned weighting, that is the product of the weighting of all intermediate branches in the path from the root to the terminal node. Theoretically, the number of branches can be arbitrary, although there is little point in increasing the complexity too much, because the influence on the output becomes minimal for small weightings $< 10\%$. The respective weightings have to be determined on the basis of the credibility of the scenario represented by the respective branch or on the relative confidence of the analyst group.

5. Seismicity Model

In order to perform a probabilistic seismic hazard assessment based on Cornell (1968) and McGuire (1976) the seismicity along the Vanuatu island arc has to be subdivided into source zones with homogenous earthquake activity. These source zones serve two purposes: (1) to adequately represent the geological and tectonic setting together with the recorded seismicity, and (2) to allow for expected variations in future seismicity. The latter aspect is obviously associated with considerable epistemic uncertainty due to our incomplete understanding of the tectonic setting. In order to allow for different projections of future seismicity based on different interpretations of the available data, we developed three alternative set of source zones, from now on referred to as seismicity models. The construction of these three zonation schemes representing the epistemic uncertainty is described below.

5.1 Seismicity distribution

At first sight, the seismicity along the Vanuatu subduction zone seems to be evenly spread. But a closer look reveals a more complex and strongly depth-dependent pattern (cf. Figure 5.1). It is generally not reasonable to account for all these complexities in the zonation because the source zones would become to small. Marginal source zones are problematic for two technical reasons: (1) insufficient data impedes the reliable estimation of the seismicity parameters, and (2) the fracture area of the earthquakes cannot exceed the size of their source zone. Therefore, we construct three models with variably detailed zonations for the three depth ranges: shallow ≤ 60 km, intermediate $60 - 120$ km and deep > 120 km.

The main question in the definition of these seismicity models is the interpretation of slab anomalies discussed in the following Section 5.1.1: The area of quiescence could be interpreted as an inactive or formerly active fault. In that case, the future activity will most probably remain low and so will the seismic hazard. But in an alternative second scenario the low activity could have led to an accumulation of tensions, that might be released in a seldom but major event. If that was the case, the expected hazard in this area would change its characteristics with respect to the adjacent regions with a more regular seismicity.

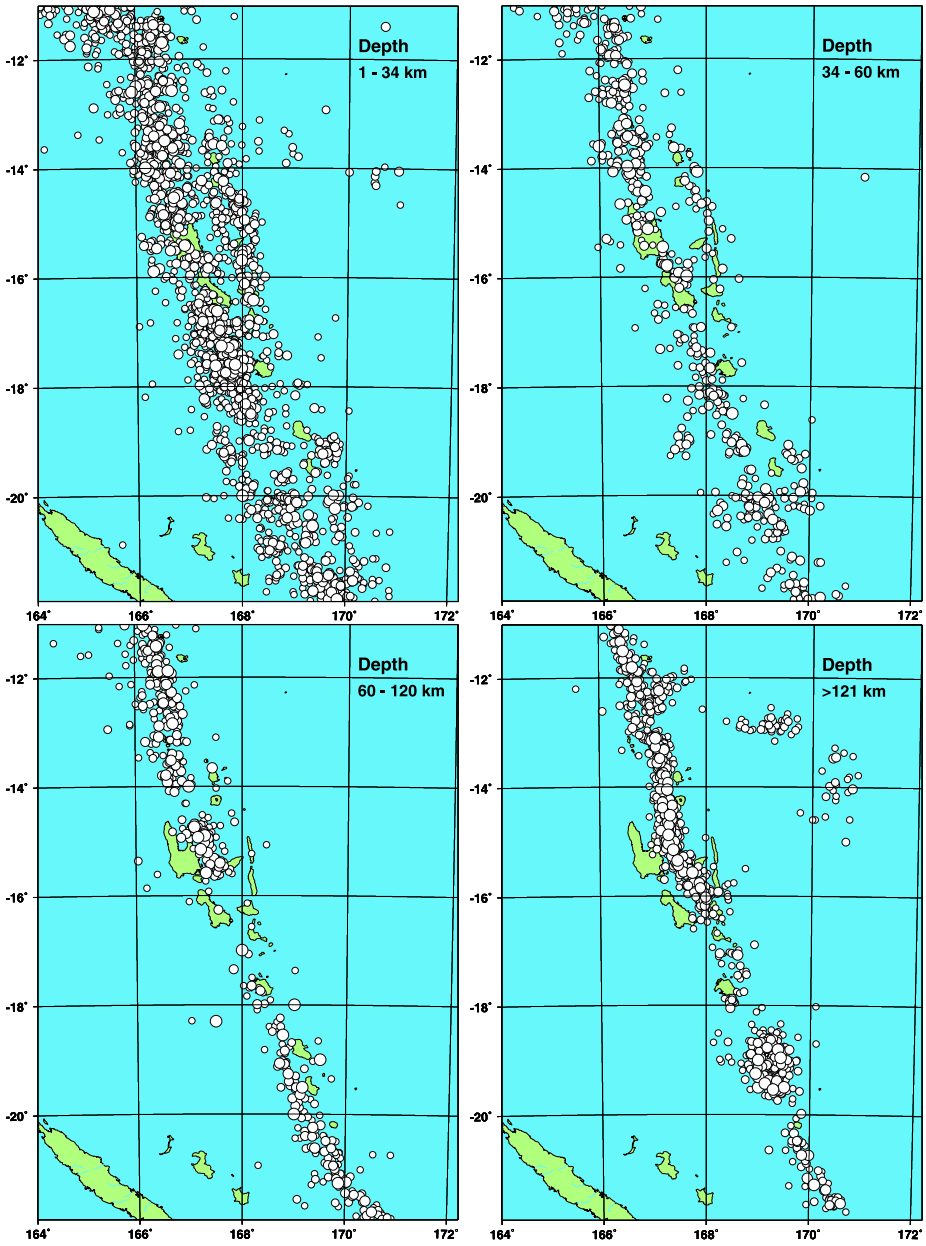

Fig. 5.1: The four figures display the epicentres of earthquakes with $M_w \geq 5$ occurring in the respective depth ranges : $1 - 34$ km (upper left), $34 - 60$ km (upper right), $60 - 120$ km (lower left) and > 120 km (lower right). The indicated radii correspond to the magnitude of the event as in Figures 3.1 and 3.2. The most striking irregularity occurs in depths > 60 km, where an extremely low seismicity rate can be observed in the central region. The subduction is much clearer defined in deeper depths, backarc activity seems limited to shallow areas.

5.1.1 Slab anomalies

The most striking irregularity in the subducting slab occurs in the central part of the Vanuatu island arc. In this area earthquake locations from both worldwide and local networks (Prévot et al., 1991) show a sizable gap in the Wadati-Benioff zone. The depth profile of the subduction is plotted in Figures 5.2. The low activity rate for depths below 60 km in area 4 stands out particularly clearly. This observation corresponds to the distribution of epicentres in Figure 5.1 for the area around Efate and Epi.

Previous authors (Chatelain and Grasso, 1992; Chatelain et al., 1993; Choudhury et al., 1975; Louat and Pelletier, 1989) have interpreted this feature as evidence for a detachment of the middle segment of the lower part of the down-going slab. Prévot et al. (1994) proposed the existence of a shallow double seismic zone within the descending Australian plate beneath the central part of Vanuatu. They claim that the distance between the upper and lower levels is $50 - 70$ km and that they are joined at 80 km depth by a near-horizontal band of seismicity.

5.1.2 Spatial seismicity variations

Two additional irregularities in the seismicity distribution are apparent in Figure 5.1. First, the subduction emerges much clearer in the deep depth ranges $60 - 120$ km and > 120 km. In the shallow areas it is more dispersed, partly because of the smaller dip angle of the slab, partly due to the existence of other seismic sources. These are: backarc trenches, volcanic activity and active faults on the arc platform. Second, the backarc activity seems to be limited to shallow depths above 60 km (see also Figure 5.2). Most of the backarc seismicity occurs in the central area around $-14°$S to $-16°$S, roughly where the D'Entrecasteaux ridge enters the subduction and is mainly related to the central backarc trench (Pelletier et al., 1998) plotted in the tectonic map (Figure 2.2 in Chapter 2).

The existence of active faults or asperities on the arc platform is more controversial. In the course of the Ocean Drilling Program, Greene et al. (1994) reported several active faults on Espiritu Santo and Malekula. Other authors (Meffre and Crawford, 2001), however, could not confirm these observations. Based on the data available to us we decided to only explicitly include the central backarc as a separate source zone, because there can be no doubt about considerable seismic activity in that area.

5.2 Definition of seismic source zones

According to the above considerations the Vanuatu island arc is divisible in three ways: from up to down into different depth ranges, from west to east into areas with

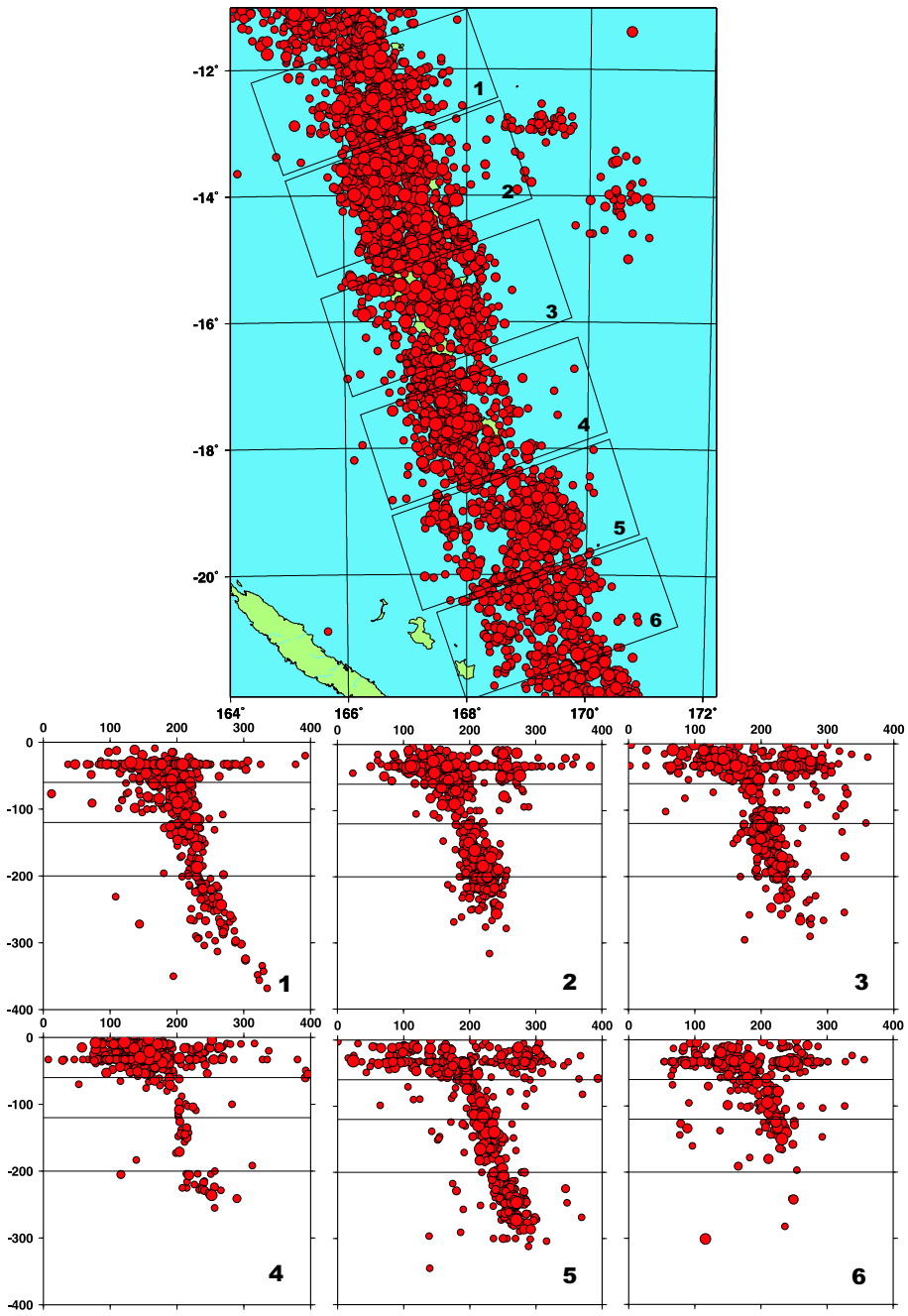

Fig. 5.2: The above six depth profile show the devolution of the subducting slab along the Vanuatu island arc. The six areas are outlined on the epicentre map on top and numbered from north to south. For the below diagrams, all events were projected onto a common plane perpendicular to the subduction. The x-coordinate denotes the focal depth of the events and the y-coordinate their distance from the western edge of the respective segment. The horizontal lines at 60, 120, and 200 km depth indicate the three ranges common to all three seismicity models. Displayed are only those globally registered events with $M_w \geq 5$. The coverage of the local network is not sufficient to allow a comparison of the spatial distribution of seismicity along the entire archipelago.

specific seismic sources, and from north to south into geologically diverse segments of the slab. These classifications can be summarised in the following way.

From up to down there are three depth ranges (indicated in Figure 5.2):

1. The shallow depth range $0-60$ km with relatively homogenous seismicity along the subducting slab, as well as backarc and volcanic activity particularly in the central area;

2. The intermediate depth range $60-120$ km with high seismic activity in the clearly defined northern and southern trench and a seismic gap in the central area;

3. The deep depth range >120 km with a higher seismicity rate but a generally similar spatial distribution than in the intermediate depth.

In certain areas the seismicity in Vanuatu extends to 700 km in depth. Apart from the lower part of the subducting slab some very deep earthquakes have been recorded in the Fiji basin, which corresponds to the upper-right corner on the maps in Figure 5.1. However, it is neither necessary (the contribution of very deep events to the acceleration at the surface is negligible) nor possible (due to anomalies in the treatment of deep events in the attenuation used, see Chapter 6) to take all these extremely deep events into account.

The depth classification is common to all three seismicity models. The west-to-east zonation varies slightly with the only difference being the aggregation of the volcanic chain and the backarc activity in the third, coarsest model. The colouring in Figure 5.3 clarifies the distinguished areas. These are from west to east:

1. A zone of diffuse seismicity that cannot be clearly assigned to a specified seismic source - possibly including erroneous localisations (light yellow areas in Figure 5.3);

2. The subducting slab dominating seismic activity in Vanuatu (orange);

3. The backarc (and the volcanic chain in the central part) with a shallow but considerable seismicity (yellow); and

4. Another zone of diffuse seismicity in the North Fiji basin (light yellow).

The three alternative models mainly differ in their zonation of the subducting slab from north to south, which is based on the neotectonic analysis in chapter 2. The most detailed zonation would be the following (again, see the left map in Figure 5.3), from north to south:

1. The northern segment just south of where the subduction changes direction, becoming the Solomon Island arc;

2. The zone where the West Torres plateau is being subducted;
3. The area around Espritu Santo and Malekula which is dominated by the collision of the D'Entrecasteaux ridge;
4. The part around Efate which is characterised by irregularities in the large depths;
5. The southern segment just off Erromango and Tanna with homogenous activity;
6. The part in the vicinity of the Loyalty islands ridge.

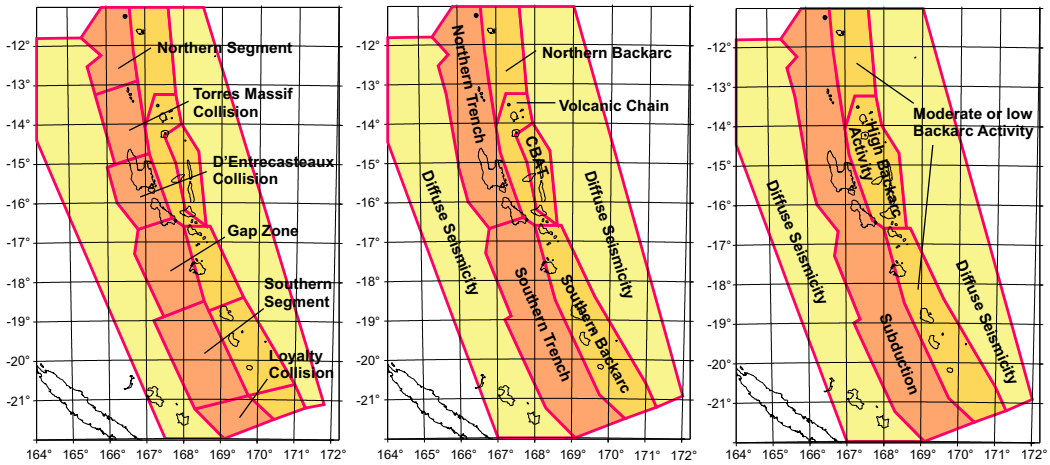

Fig. 5.3: The three figures show the zonation in the shallow depths range $(0 - 60$ km) for the three different seismicity models: the detailed (left), the intermediate (middle), and the coarse model (right). The colouring indicates the west-east division of the area into zones of diffuse seismicity (light yellow), subduction seismicity (orange), and backarc activity (yellow). This classification is common to all three models. While the detailed model divides the archipelago into blocks of 200 km, the intermediate model retains only the distinction between northern and southern trench, and the coarse model treats the subduction as one homogenous zone. (Note that the abbreviation CBAT in the middle model refers to the Central Back-Arc Trench.)

These zones divide the island arc into blocks of approximately 200 km. Since for technical reasons, the fracture area of earthquakes cannot exceed the size of their source zone, it is not advisable to reduce the source zones further. Figure 5.3 shows the two generalisations made in the additional two seismicity models. The intermediate model only retains the division into a northern and southern trench (thereby

implicitly assuming that majors events will not take place in the central area), and the coarse model considers the whole subduction as one zone. In that case the seismicity rate is considered uniform along the entire arc. Although this assumption is not realistic, it is important to account for the possibility of an earthquake fracturing the entire arc. The weight assigned to this respective seismicity model is chosen appropriately low.

5.2.1 Characterising the seismicity

The seismicity in each source zones is characterised by: the Gutenberg-Richter parameters a and b defined through the well confirmed magnitude-frequency relation (Gutenberg and Richter, 1944):

$$\log N = a + bM, \tag{5.1}$$

the maximum expected magnitude and the expected focal depths. In (5.1) N is the number of earthquakes with magnitude M. The maximum expected magnitude M_{max_i} for the specific source zone i and a minimum magnitude M_{min_i} below which significant damage will not occur, usually truncate the distribution (see Figure 5.4). Since the source zones of the detailed seismicity model do not contain sufficient data in some source zones to perform regressions, we aggregate zones for the estimation of b-values only. The criteria for the aggregation are that (1) the source zones lie in the same depth range and (2) that they have comparable seismicity. The zones of diffuse seismicity are an exception in the sense that they are aggregated over different depth ranges. This is inevitable since very few events are recorded in these zones and because their low activity is distinctively different from the rest of the island arc. The quality of the regressions in the areas of diffuse seismicity is nonetheless rather poor.

Due to the aggregation of source zones, we obtain homogenous b-values for those source zones that subdivide the subduction (varying in the interval $0.65 \leq b \leq 0.75$). For the zones of diffuse seismicity that flank the subduction, the b-values increase considerably to $1.58 \leq b \leq 1.62$. A more comprehensive list of the Gutenberg-Richter parameters for the detailed seismicity model is given in Appendix C.

In prior estimates, Acharya (1971) and Hofstetter et al. (2000) found similar b-values for shallow depths, but considerably smaller b-values for deep depths: Acharya (1971) estimated a maximum b-value of 0.81 in shallow depths and b-values as low as 0.48 for earthquakes exceeding 300 km focal depth. Note that contrary to both Acharya (1971) and Hofstetter et al. (2000) we calculated b-values using mainshocks only.

Apart from the Gutenberg-Richter parameters a and b, it is common to use the parameters α and β to calculate the annual rate of earthquakes $\nu(M_{min})$ exceeding

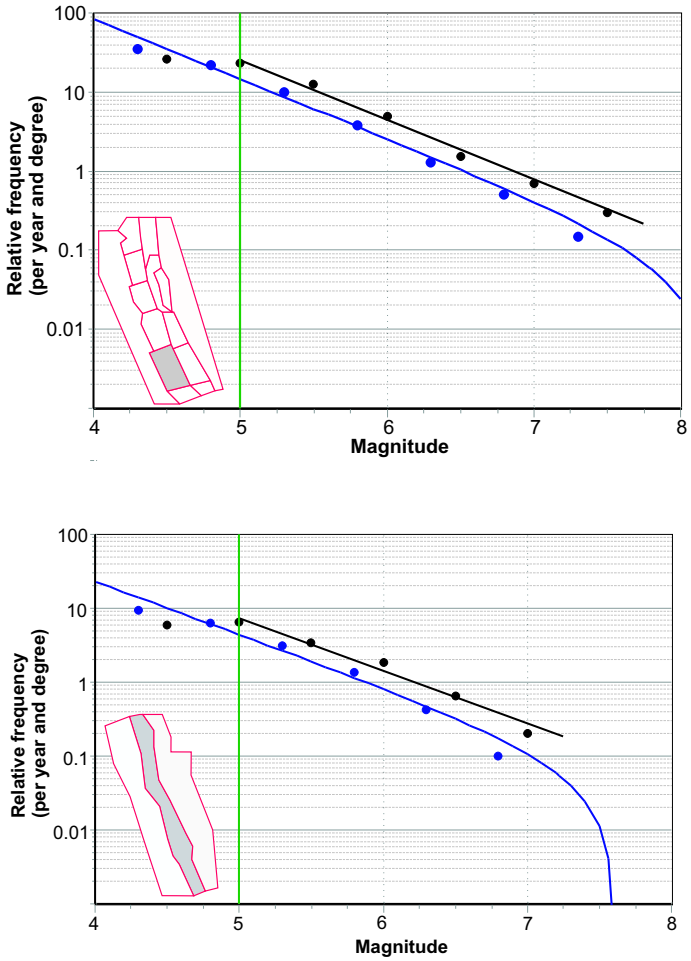

Fig. 5.4: The figures show magnitude-frequency relations for two exemplary source zones: the Southern Block in shallow depths ($0 - 60$ km) from the detailed model (top) and the deep subduction zone ($120 - 200$ km) from the coarse model (bottom). The zonation scheme for the respective depth and seismicity model is displayed in the lower left corner of the diagram with the investigated zone shaded in grey. The frequency of events within each magnitude class (in steps of 0.5 magnitude units) is indicated in black, the cumulative frequency in blue (consequently, the frequency is plotted in the centre of the magnitude class, the cumulative frequency at the lower border of the magnitude interval). The two fits (for events with $M_w \geq 5$) are coloured accordingly. The minimum magnitude for the fit was set to ($M_w = 5$) and is marked by a green line. In the Southern Block (upper diagram) 175 events were used in the fit and yield the b-value: $b = 0.710(\pm 0.023)$; in the deep subduction zone (bottom diagram) 588 events were utilised to determine the b-value: $b = 0.751(\pm 0.032)$.

the minimum magnitude M_{min}. The relation between these parameters is given by:

$$\nu(M) = \exp(\alpha - \beta M) = 10^{a-bM} \tag{5.2}$$

In this study we set the minimum magnitude to $M_{min_i} = 4.5$ for all zones. This choice is motivated by the data available, by the presumption that earthquakes below moment magnitude $M_w = 4.5$ cause negligible damage and of course by the limitations of the used attenuation relations (see Section 6) with respect to M_{min}. We therefore characterize the annual rate of earthquakes at this magnitude $\nu(4.5)$. In our calculation we use $\nu(4.5)$ instead of the also common a-value. See Appendix C) for a complete list of $\nu(4.5)$-values for the detailed seismicity model.

The determination of the maximum expected magnitude is based on the events that have occurred in that zone. But the maximum observed magnitude M_{obs} is only a lower bound for the maximum expected magnitude due to the limited observation period. For the logic tree we will therefore consider three possibilities for the maximum expected magnitude: $M_{max1} = M_{obs} + 0.25$, $M_{max2} = M_{obs} + 0.5$, and $M_{max3} = M_{obs} + 0.75$.

The expected focal depths in each zone are determined through two criteria: the chosen depths should reflect the general distribution of events (see Figure 4.2) and the depths with the highest frequency of major earthquakes should be considered. A full characterisation of the seismicity for the detailed zonation scheme is given in Appendix C.

6. Attenuation Relations

We selected four recent attenuation relations for our seismic hazard calculations. The criteria for the selection were (1) whether or not the attenuation relation was developed using subduction zone data, (2) which data sources were used for the derivation, (3) the explicit inclusion of focal depth as a variable, (4) that the attenuation relation extended to high enough magnitudes, and (5) that the set of chosen relations should reflect the diversity of available expertise concerning attenuation.

Applying the four chosen approaches in our study yielded highly varying results for the expected peak ground acceleration (PGA) associated with the same event parameters. A more detailed analysis showed that the main deficiency of the approaches is the treatment of focal depth. This observation forced us to further limit the depths range of the considered events. Overall, the attenuation models introduce the major bias to this hazard analysis.

6.1 Four approaches to model attenuation in subduction zones

The approaches by Youngs et al. (1997) and Crouse (1991) are based on the same functional form with the difference that Youngs et al. (1997) additionally differentiates between interface and intraslab earthquakes. Interface events usually occur in shallow depths at the interface between the subducting and the overriding plate. Contrary, intraslab earthquakes take place within the subducting plate and are thought to respond to downdip tension in the subducting plate (Youngs et al., 1997). Due to incomplete information about the focal mechanisms of earthquakes in Vanuatu, we use the focal depth as a criterion whether the event is classified as interface or intraslab. This procedure was adopted from Youngs et al. (1997). We will assume that events in the shallow depths range ($0 - 60$ km) are generally interface earthquakes. Furthermore, we expect that the majority (80%) of deep events (focal depths > 60 km) have an intraslab mechanism and only 20% one of interface type.

The ground motion models by Takahashi et al. (2000), and Lussou et al. (2001) have been selected because they are deduced from the records of the Kyoshin network monitored by the National Research Institute for Earth Science and Disaster Prevention, Japan, which is one of the best strong motion networks in an active subduction zone. Both of the latter relations predict significantly smaller PGAs than

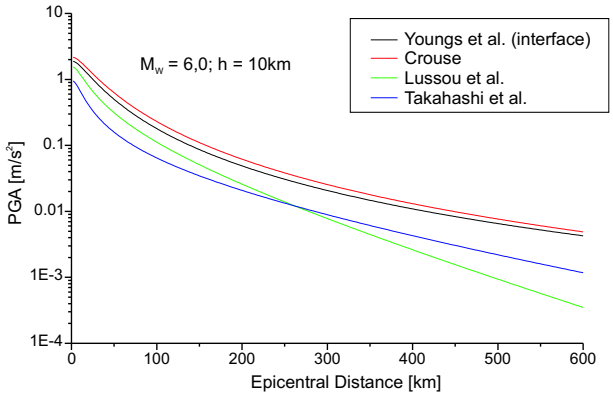

Fig. 6.1: The peak ground accelerations (PGA $\left[\mathrm{m/s^2}\right]$) on a logarithmic scale caused by an earthquake with $M_w = 6.0$ at 10 km depth as expected by the four attenuation relations: Youngs et al. (1997) (interface mechanism), Crouse (1991), Takahashi et al. (2000), and Lussou et al. (2001) for different distances ($0-600$ km) to the epicentre. The anticipated ground motions vary significantly – above all in their rate of decay with distance.

Youngs et al. (1997) and Crouse (1991), cf. Figure 6.1. The important restriction is that the attenuation relations by Takahashi et al. (2000) and Lussou et al. (2001) are only applicable in shallow depth ranges.

6.1.1 Ground classification

The attenuation of seismic ground motion at a specific site depends strongly on the soil conditions. This dependence is usually accounted for through a site classification based on the shear wave velocity. Unfortunately, there are no consistent norms for these classifications. Takahashi et al. (2000) and Lussou et al. (2001) consider four classes: rock, hard soil, medium soil and soft soil, while Youngs et al. (1997) only discriminates between rock and soil. The Vanuatu island arc is of volcanic origin and therefore we consider either one of the categories rock and stiff soil to be most realistic. The seismic hazard is calculated for both soil types. Generally, ground accelerations caused by a specific event are expected to be higher for soil than for rock conditions (cf. Figure 7.3). By considering the two classes, we thus obtain and upper and a lower bound estimate with the actual PGA lying in between. Nonetheless, we consider the rock category to be closer to the actual situation for most sites and the values resulting from it as closer to reality.

6.2 Systematic Inadequacies

For various reasons we argue that none of the described attenuation relations is applicable over the whole range of seismicity data in Vanuatu. Takahashi et al. (2000) and Lussou et al. (2001) both restricted their analysis to shallow events. Accordingly, we use their attenuation relations only in our hazard calculations for the shallow depths range $0 - 60$ km.

Crouse (1991) originally derived his attenuation model in order to estimate the expected ground motion of earthquakes on the Cascadia subduction zone. Contrary to Youngs et al. (1997), he does not comment on the transferability of his model to other subduction zones.

Youngs et al. (1997) claims that his relation appropriately describes the attenuation for subduction zone interface and intraslab earthquakes of moment magnitude $M_w \geq 5$ for distances of 10 to 500 km. However, his data set contains no records of very deep earthquakes. The deepest event considered occurred at a focal depths of 229 km, and only 7 earthquakes in the depths range $150 - 200$ km are taken into account for the regression analysis.

An additional difficulty arises from the fact that Youngs et al. (1997) uses the closest distance to the rupture surface as a measure of distance for his regressions. But this information is unavailable for most events contained in our catalogue for Vanuatu. Instead we use the hypocentral distance. For small events, this is an acceptable substitute. However, for large events the difference between these two measures of distance can be considerable and introduces a potentially large bias.

We therefore expect that the proposed peak ground accelerations might be problematic, particularly for remote and deep events at large magnitudes. We tested the resulting peak ground accelerations for both attenuation relations by Crouse (1991)

$$\begin{aligned} \ln(PGA_{m,r,h}) &= 6.36 + 1.76m - 2.73\ln(r + 1.58\exp(0.608m)) + 0.00916h \\ &\quad \text{with} \quad \sigma = 0.773 \end{aligned} \tag{6.1}$$

and Youngs et al. (1997)

$$\begin{aligned} \ln(PGA_{m,r,h}) &= 0.2418 + 1.414m - 2.552\ln(r + 1.7818\exp(0.554m)) \\ &\quad +0.00607h + 0.3846z_t, \\ &\quad \text{with} \quad \sigma_m = 1.45 - 0.1m \end{aligned} \tag{6.2}$$

with moment magnitude m, hypocentral distance r, focal depth h, and a focal mechanism parameter z_t, which is 1 for intraslab and 0 for interface events.

The analysis in Figure 6.2 shows that both attenuation relations overestimate the ground acceleration caused by remote deep events. Obviously, it should be expected that the ground motion caused by an earthquake (with given magnitude and

epicentral distance) at a specific site decays with the focal depth of the respective event. In Figure 6.2 this hypothesis is tested at varying epicentral distances for events with $M_w = 6$ and for the attenuation relations by Youngs et al. (1997) (left figure) and Crouse (1991) (right figure). The anticipated trend is only confirmed for sites that are sufficiently close to the epicentre ($D_{epi} = 10$). The peak ground acceleration caused by remote deep events is significantly overestimated: Comparing two $M_w = 6$ earthquakes at a fixed epicentral distance to the site under investigation, the event in 200 km depth causes higher ground motion than the one in 50 km depth. We conducted additional tests and the same problem emerges for earthquakes with interface mechanism. Part of this anomaly may be due to the fact that we are using the hypocentral distance instead of the closest distance to the rupture surface for our dataset. This simplification is apparently problematic for remote deep events with large magnitudes.

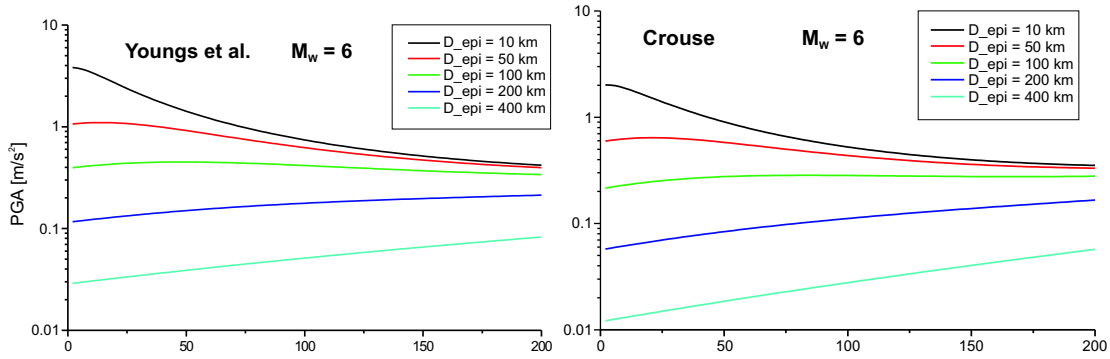

Fig. 6.2: This figure illustrates the limited applicability of the attenuation relations by Youngs et al. (1997) and Crouse (1991) for remote deep events. The left sets of curves plot the peak ground acceleration against the focal depths of the events as expected by Youngs et al. (1997) for intraslab events with magnitude $M_w = 6$. The different curves refer to different epicentral distances at which the ground acceleration is calculated ($D_{epi} = 10$ km to $D_{epi} = 400$ km). The curves on the right illustrate the same phenomenon for $M_w = 6$ events according to Crouse (1991). Graphs with corresponding epicentral distances D_{epi} are coloured accordingly in both figures. Note that due to data limitations we have to use the hypocentral distance instead of the closest distance to the rupture surface.

The subduction seismicity in the Vanuatu island arc extends down to 700 km in certain areas (cf. the analysis in Chapter 5). The earthquake catalogue thus contains a large number of the problematic type of events, namely strong earthquakes at large focal depths and large epicentral distances. As shown above, the peak ground acceleration generated by these is not adequately modeled by the chosen four attenuation

relations.

For these reasons, we decided to discard events below 200 km in focal depths. This cutoff point is motivated by the data Youngs et al. (1997) used to derive his proposed attenuation relations. As indicated above, their data included only one single event below 200 km. Moreover we expect a minor contribution to seismic hazard of these very deep events.

This left us with the question how to treat events in the depths range $120 - 200$ km. On the one hand, we cannot exclude the possibility that they contribute to the seismic hazard in Vanuatu. On the other hand, the peak ground acceleration generated by these could be biased by the described limited applicability of the attenuation relations. In order to minimize arbitrariness we chose to conduct a sensitivity analysis and created two datasets: One excluding those events with focal depths between $120 - 200$ km, the other including these events. In Chapter 7 we compare the two resulting hazard maps.

7. Seismic Hazard Calculations

The results of our seismic hazard calculations can best be depicted in two ways: (1) as seismic hazard curves or (2) as seismic hazard maps. Seismic hazard curves refer to a specific location within the investigated area. The advantage of this site-specific representation is that different hazard levels can be compared directly. Hazard maps on the other hand illustrate the spatial variation of seismic hazard within Vanuatu. They refer to a specific hazard level or mean return period - in our case 475 years which is equivalent to a 10% probability of exceedance in 50 years (cf. Chapter 4).

As described in Chapter 4 our calculations utilize the logic tree approach to account for the uncertainties associated with a probabilistic hazard assessment. Before describing our results, we summarise the specific logic tree structure adopted in our calculations. In Section 7.2 the seismic hazard curves for Port Vila are shown (cf. Figure 7.2) and discussed. The hazard maps for Vanuatu are presented in Section 7.3. We conclude with a discussion of our results and a comparison with a prior probabilistic seismic hazard assessments in the course of the Global Seismic Hazard Assessment Programme (GSHAP), where Vanuatu is part of the global seismic hazard map (cf. Section 7.4).

7.1 Logic tree

In the case of Vanuatu the general logic tree (cf. Figure 4.2) is specified as shown in Figure 7.1. The diagram refers to the shallow depths range ($0-60$ km). For the other two depths ranges, the attenuation relations by Lussou et al. (2001) and Takahashi et al. (2000) are not applicable. For these cases, the weighting of the attenuation relations is therefore replaced by 40% Youngs et al. (1997) (intraslab mechanism), 10% Youngs et al. (1997) (interface mechanism), and 50% Crouse (1991). The chosen attenuation relations and their weightings are the only difference between the logic tree for shallow and deeper depths.

The weighting of the three seismicity models implies that the seismic gap in the central region (cf. Chapter 2) is primarily (with 80% probability) considered to be an area of generally low seismicity. Apart from the numerous anomalies in the central area discussed in Section 2, a closer look at the variation of convergence rates justifies the decision to favour the actual gap concept: In the northern segment (Banks and Torres Islands) the observed convergence rate is $65-75$ mm/yr. It then

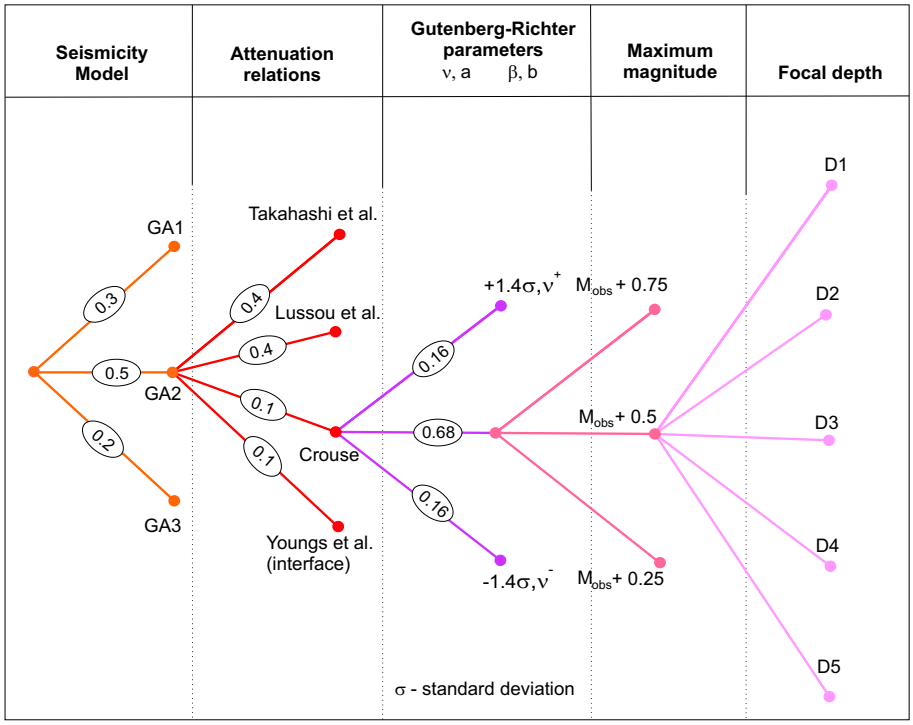

Fig. 7.1: Logic tree diagram for the shallow depth range ($0-60$ km) in reference to the general scheme in Figure 4.2. The only difference to the corresponding logic trees for the deeper areas are the attenuation relations used: 40% Youngs et al. (1997) (intraslab mechanism), 10% Youngs et al. (1997) (interface mechanism), and 50% Crouse (1991). For purposes of simplicity only a single branch is shown in detail.

rapidly decreases to $28-42$ mm/yr along the western island belt (Santo, Malekula) in the central part and to 55 mm/yr along the eastern belt (Maewo, Pentecost). A bit further south in the area around Tanna the highest observed convergence rate 124 mm/yr is reached (see also Figure 2.1).

The weighting of the magnitude-frequency parameters β and ν is based on a statistical rationale: Integrating the area below a normal distribution from $-\sigma$ to $+\sigma$ yields approximately 68% of the total area. The Gutenberg-Richter parameters are accordingly weighted with 0.68, the branches with $+1.4\sigma$ and -1.4σ with the weight of 0.16 (the factor 1.4 equals the barycentre of the area below the standardized normal distribution integrated until σ). The seismic hazard calculations have been carried out with the computer code FRISK88M© by Risk Engineering, Ltd. (1997).

7.2 Expected seismic hazard in Port Vila

Port Vila is the capital of Vanuatu and the largest city in the country. It is struck by earthquakes on a regular basis, some of which caused damage to both buildings and infrastructure. The most recent example was the earthquake on January 2nd, 2002. A description of the event and a comprehensive assessment of the damages can be found in the SOPAC report (Garaebiti et al., 2002).

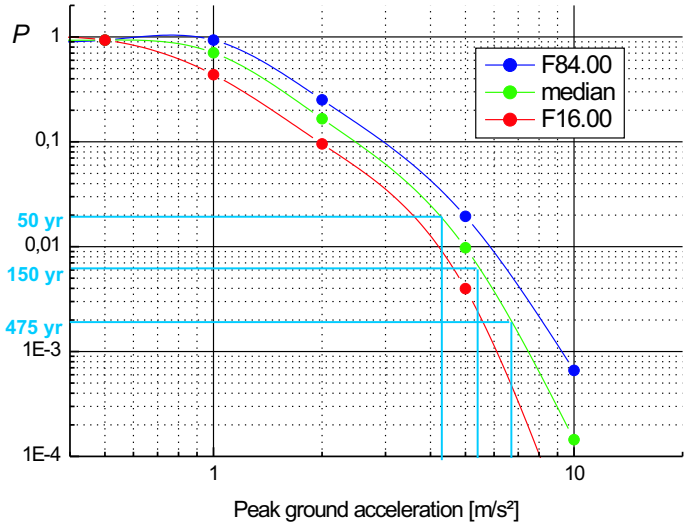

Fig. 7.2: The three curves specify the seismic hazard P in Port Vila. The seismic hazard is plotted over the peak ground acceleration given in m/s^2. Three specific hazard levels, expresses here as mean return periods T, are indicated in blue: $T = 50$ yr, $T = 150$ yr, and $T = 475$ yr.

The seismic hazard curves for Port Vila (the coordinates were set to 168.35°E 17.70° S) was calculated assuming stiff soil conditions (see Figure 7.2). The frequency of earthquake occurrence $P = \frac{1}{T}$ (where T denotes the return period) is plotted over the peak ground acceleration (PGA) given in m/s^2. Three specific recurrence periods are indicated in blue: $T = 50$ yr, $T = 150$ yr, and $T = 475$ yr. The corresponding peak ground accelerations are listed in the table below.

Mean return period T in yr	**50**	**150**	**475**
Median PGA in m/s^2	4.1	5.2	6.4

The three curves in Figure 7.2 represent the median, the median $+1\sigma$- and the median -1σ-values also referred to as fractiles; i.e. the 16% fractile is identical to

the median$-\sigma$-graph, the 50% fractile to the median graph, and the 84% fractile to the median$+\sigma$-graph. The degree to which these curves deviate from each other is a measure for the variance of resulting peak ground accelerations. The uncertainty of the estimate increases with longer return periods. Although the deviations between the three curves might seem quite high, they lie fully within the usual range for comparable studies.

7.3 Seismic hazard maps

Several hazard maps are presented in this section. All of these were calculated using global data provided by the United States Geological Survey USGS/NEIC and Engdahl et al. (1998). The hazard values are calculated on a 0.1° grid. The respective hazard maps differ in the assumed site conditions and in the treatment of deep events (cf. Figures 7.3 and 7.4).

7.3.1 Comparison of seismic hazard for different soil types

Most islands in Vanuatu are of volcanic origin. Volcanic deposits, eruptive rocks and ash layers prevail in the subsoil. Depending on the exact position, the ground can be classified either as rock or as stiff soil. However, we suppose that stiff soil is more appropriate for most sites along the Vanuatu archipelago.

The expected ground motion depends strongly on the soil conditions at the site under investigation. Generally, the acceleration experienced at soil sites is higher than for rock environments. The hazard maps in Figure 7.3 confirm this expectation: For rock conditions, the expected peak ground acceleration with a 10% probability of exceedance in 50 years varies in the interval $5 - 6.5$ m/s^2, for soil conditions the corresponding acceleration lies within the much larger interval $5.5 - 8$ m/s^2.

7.3.2 Comparison of the hazard for different depths ranges

As explained in Section 6.2, two hazard maps are calculated for both site conditions (cf. Figure 7.3): One excluding those events with focal depths below 120 km, the other including these events. This sensitivity analysis shows that the inclusion of the depth range $120 - 200$ km has a significant impact on the expected peak ground acceleration for both site conditions (cf. Figure 7.3).

In the case of stiff soil, a maximum peak ground acceleration of approximately 7.6 m/s^2 is reached in the east of Espiritu Santo if events with focal depth $0 - 200$ km are considered. If those in the range of $120 - 200$ km are neglected, the maximum expected peak ground acceleration decreases to roughly 6.6 m/s^2 for the same area. For rock conditions, the situation is analogous.

We pursued the same comparison for other islands along the Vanuatu island arc and found that the following rule-of-thumb holds: the inclusion of events in the depth range $120 - 200$ km increases the expected peak ground acceleration by roughly 1 m/s^2. The spatial distribution of seismic hazard is virtually unaffected by the inclusion of events in the questionable depth range $120 - 200$ km.

The range of uncertainty in the resulting hazard is shown in Figure 7.4, where the maps for rock conditions are shown for the median (50% fractile), the median $\pm 1\sigma$ standard deviation (84% and 16% fractile) as well as far the mean values. Due to the obliqueness of the resulting values in the range of fractiles, the mean deviates usually significantly from the median.

7.4 Conclusion

This last section is devoted to a summary and critical discussion of our results. We compare our hazard assessment to prior estimates obtained in the course of GSHAP. We also give a brief outlook on further research that would improve the assessment of seismic hazard further.

7.4.1 Summary of main results

The hazard maps in Figure 7.3 are the main result of our study. The median values for seismic hazard are displayed for two different site conditions (rock and stiff soil) and for two different depth ranges ($0 - 120$ km and $0 - 200$ km). Of these four maps, we consider the one for stiff soil and the depth range $0 - 200$ km (cf. bottom figure on the left in Figure 7.3) to best quantify the ground motion in Vanuatu (with a 10% probability of exceedance in 50 years). The rationale for that choice is: (1) We think that the site category "stiff soil" tends to describe the Vanuatu island arc more adequately than rock conditions. (2) We cannot rule out the possibility that an earthquake below 120 km focal depth causes notable ground motion on the surface. Consequently, the events in the depth range $120 - 200$ km should be included into the hazard assessment.

Concluding we claim that the hazard map (left bottom figure in Figure 7.3) is a conservative assessment of seismic hazard in Vanuatu with a mean return period of 475 years. The map indicates that the highest ground motion is expected in eastern Espiritu Santo (cf. Figure 2.1 for an overview of the islands in Vanuatu). Peak ground accelerations of 7.6 m/s^2 can be reached in that area. However, with expected peak ground accelerations in the range of $7.1 - 7.5$ m/s^2, the islands north of Epi are similarly affected. The lowest seismic hazard is found in the east of Efate (PGA $\approx 6.4\,\mathrm{m/s^2}$). Despite these variations, the entire Vanuatu island arc experiences a high and quite rather homogenously distributed seismic hazard.

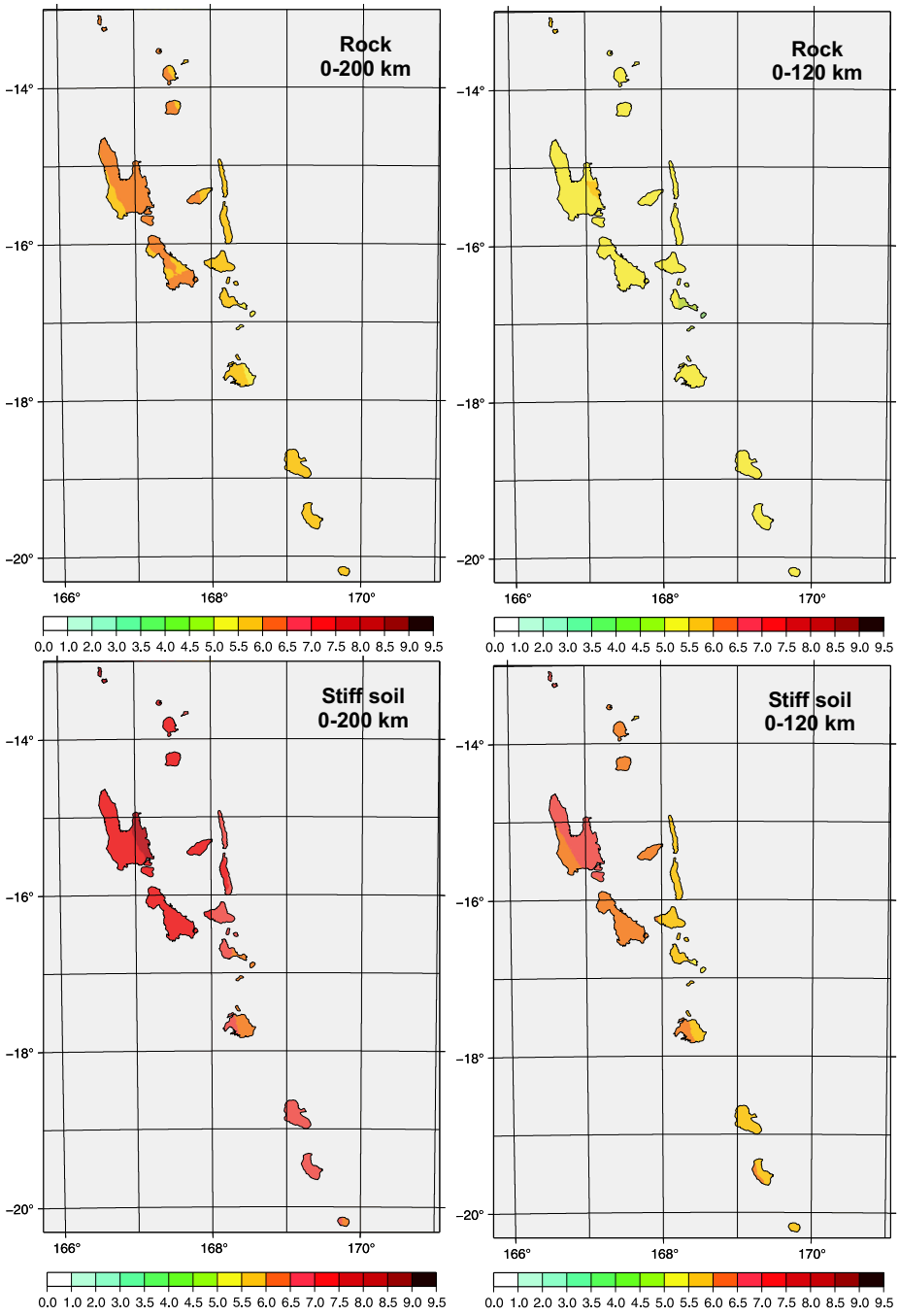

Fig. 7.3: These four maps show the medians of the predicted peak ground acceleration in m/s^2 with a 10% probability of occurrence or exceedance within 50 years. The upper left figure is calculated for rock sites considering all three depths ranges ($0-60$ km, $60-120$ km and $120-200$ km), the upper right figure also refers to rock sites, but neglects the events below 120 km due to the problematically high ground motion predicted for deep and remote events discussed in Section 6.2. Accordingly, the bottom left figure is calculated for stiff soil and all depths, and the bottom right figure for soil and depths until 120 km.

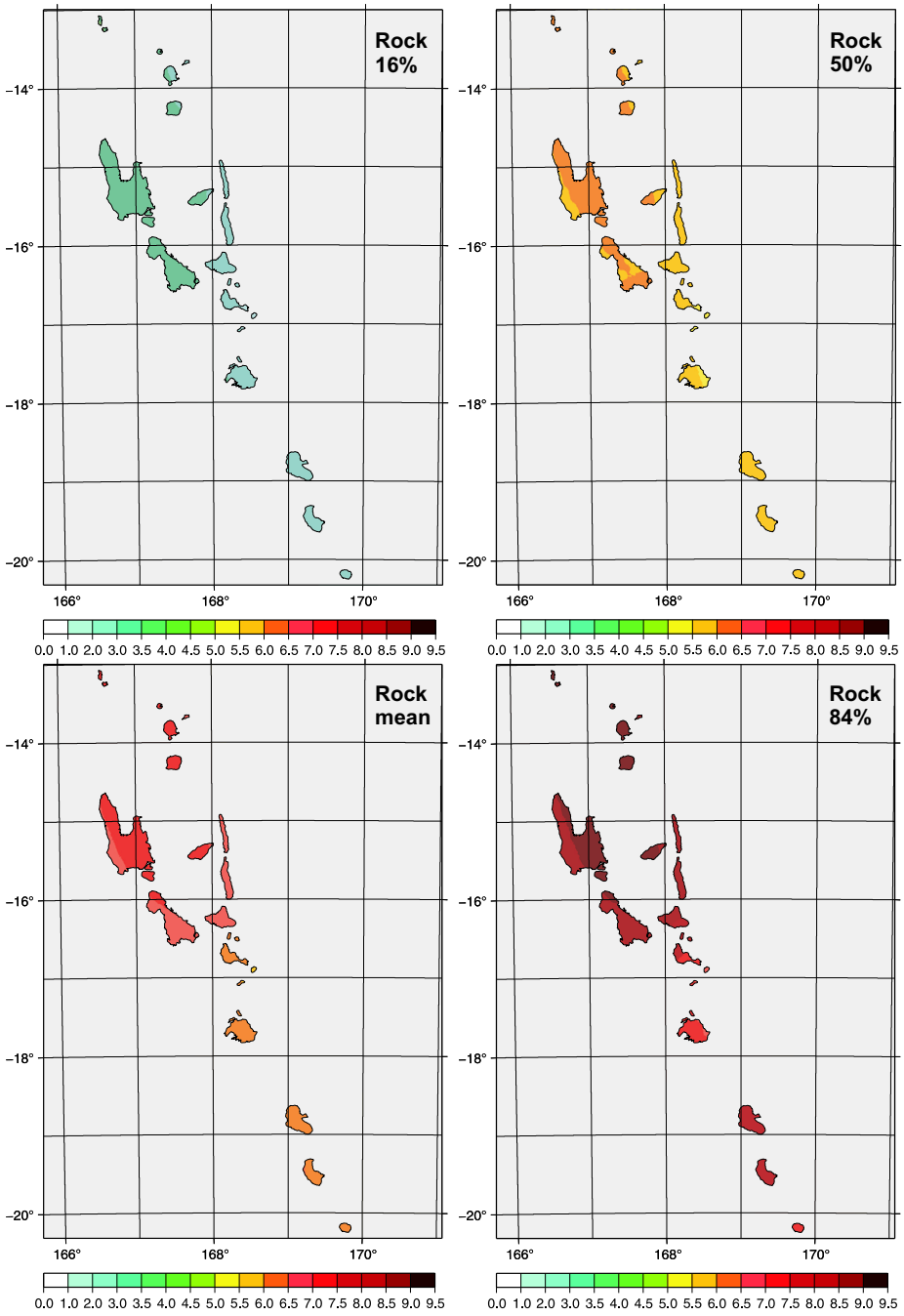

Fig. 7.4: The four figures show different fractiles: 16% (upper left), 50% median (upper right), mean (bottom left), and 84% (bottom right) of the expected peak ground acceleration m/s^2 with a 10% probability of occurrence or exceedance in 50 years (475 yr mean return period) for rock sites and focal depths of $0 - 200$ km. The fractiles quantify the variance inherent in probabilistic assessments. Although the differences between the four might seem quite high, they lie within the usual range for seismic hazard studies and are mainly due to the aleatoric uncertainties of the attenuation relations.

7.4.2 Comparison with prior estimates

The Global Seismic Hazard Assessment Programme (GSHAP; Shedlock et al., 2000) provides seismic hazard estimates for Vanuatu for the same hazard level of 10% occurrence or exceedance within 50 years (cf. Figure 1.1) as it is subject of this study. McCue (1999) provided the GSHAP results for Australia, New Zealand, the South Pacific Islands for this global project. When the results of this global project will be considered for comparison with detailed studies like the one we are presenting here, one has to take into account that the global project, based entirely on volunteer contributions, never aimed at to be as precise as local studies can be. The challenge of GSHAP was to come up with a global map based on a more or less homogeneous methodology and to invite more detailed regional, sub-regional and local seismic hazard studies. Both results, i.e. those from McCue (1999) and ours, are compared to our own results in Figure 7.5. Note that the colour scale has been adopted to better reflect the variations in seismic hazard in Vanuatu and is not the same as in Figure 1.1 with the colour code originally used for the GSHAP map. The used colouring is consistent with the hazard maps shown so far. This detailed colouring of the GSHAP-map data is possible on the basis of the GSHAP internet presentation of the GFZ Potsdam (http://seismohazard.gfz-potsdam.de/projects/en/gshap/menue_gshap_e.html) as one of the main contributors to this project (Grünthal et al., 1999a,b) where the detailed data set of this map can be downloaded.

According to our calculations, the expected PGA values are relatively small in the frame of the study conducted within the Global Seismic Hazard Assessment Program. We calculated significantly higher peak ground accelerations with less spatial variations along the island arc. The deviation of our estimates from those made within GSHAP is particularly high for the islands north of Epi and east of the Aoba basin. In these areas we expect peak ground accelerations to be approximately $4 - 5$ m/s^2 higher than shown in the GSHAP hazard map. However, one important caveat exists: the seismicity in the concerned areas is dominated by deep subduction zone events and backarc activity and is therefore prone to be affected by systematic errors in the modeling of attenuation. Nonetheless, we expect the potential error to be small: Our analysis of the contribution of the depth range $0 - 120$ km in Figure 7.3 confirmed that these do not alter the spatial distribution of seismic hazard.

The hazard maps for New Zealand (Stirling et al., 2002) show much stronger spatial variations as those for Vanuatu with obtained peak ground accelerations of up to 10m/s^2 for a 475 years mean return period. These rather high values are only reached in a small area directly on the South West Alpine fault. Other detailed PSHA are, accordingly to our knowledge, lacking for other parts of the South Pacific region.

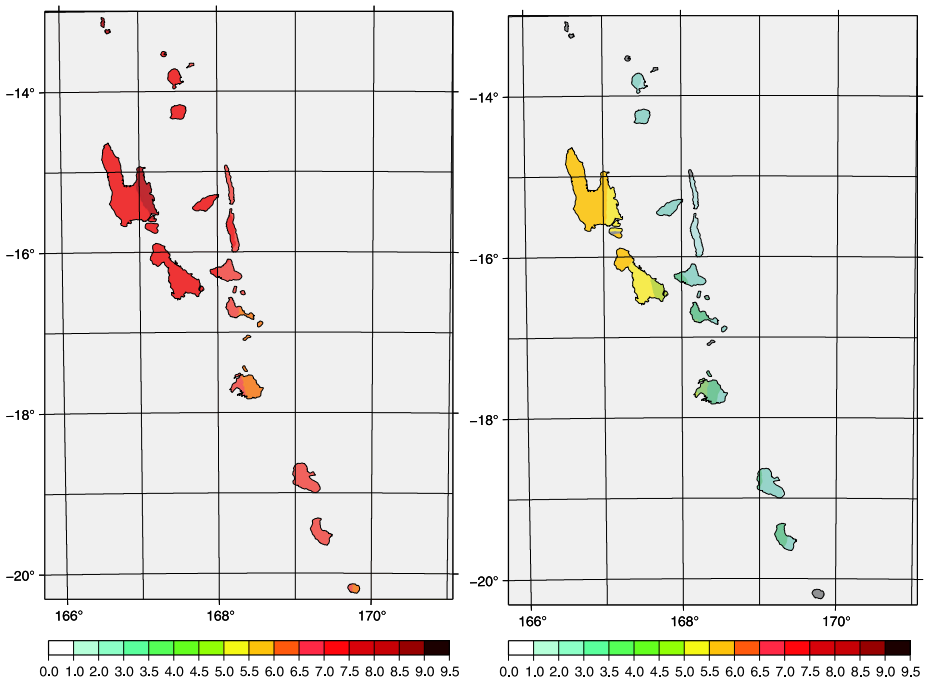

Fig. 7.5: The hazard map on the right is a detail of the GSHAP world map by Shedlock et al. (2000). Note that the colouring of the GSHAP map as shown here differs from the one chosen for the world map in Figure 1.1. Note that both hazard maps refer to a 10% probability of exceedance in 50 years (or equivalently: a 475 yr return period). The hazard map on the left shows the median peak ground acceleration in m/s^2 for stiff soil sites and the depth range $0 - 200$ km. According to our analysis, the seismic hazard was underestimated by GSHAP. We expect generally higher peak ground accelerations and less spatial variations, indicating that entire Vanuatu is prone to high seismic hazard.

7.4.3 Discussion

Our paper presents the first detailed seismic hazard analysis for Vanuatu. Within the global seismic hazard project (GSHAP), where Vanuatu was part of this rather rough earlier estimates, lower ground accelerations were provided. With respect to our study, two important caveats remain: First, the available attenuation relations are not applicable to all events contained in our catalogue. Consequentially, we had to restrict our dataset to events above 200 km in focal depths. However, deep earthquakes (down to almost 700 km focal depths) are partly characteristic for the seismicity in Vanuatu. The peak ground acceleration generated by events in the depths range $120 - 200$ km is also potentially biased. Further research should be devoted to explicitly consider these issues. In particular, it would be important to

calculate spectral ordinates on the basis of refined, regionally specific attenuation relations.

Second, the identification of earthquake clusters in shallow depths (above 60 km) based on magnitude-dependent windows may be problematic. Although the obtained set of independent earthquakes is Poisson distributed, the algorithm tends to identify too many dependent events (as suggested by Reasenberg (1985)). A more thorough understanding of aftershock activity would be desirable to develop a more appropriate de-clustering technique.

Finally, the inclusion of the local catalogues may lead to new insights into our hazard assessment. Due to statistical problems related to their limited coverage, it was impossible to include the local catalogues at this point. However, it may be possible to consider these catalogues at least for the calculation of revised hazard curves for Port Vila. In this context it would also be interesting to try to consider the findings of the microzonation study by Regnier et al. (2000) by applying the methodology by Parolai et al. (2005 (submitted)) which directly incorporates microzonation features in the probabilistic seismic hazard assessment. However, this task clearly exceeds the scope of this report.

Appendix

A. Abbreviations

AGSO	Australian Geological Survey Organisation
CBAT	Central Back-Arc Trench
DGMWR	Department of Geology, Mines, and Water Resources, Vanuatu
GFZ	GeoForschungsZentrum Potsdam
GPS	Global Positioning System
GSHAP	Global Seismic Hazard Assessment Programme
IRD	Institut de Recherche pour le Développement
M_C	Coda magnitude
M_L	Local magnitude
M_S	Surface magnitude
M_w	Moment magnitude
NEIC	National Earthquake Information Center
NOAA	National Oceanic and Atmospheric Administration
ORSTOM	Office de la Recherche Scientifique et Technique Outre-Mer
PGA	Peak Ground Acceleration
PSHA	Probabilistic Seismic Hazard Assessment
SOPAC	South Pacific Applied Geoscience Commission
USGS	United States Geological Survey

B. Regressions for magnitude conversion

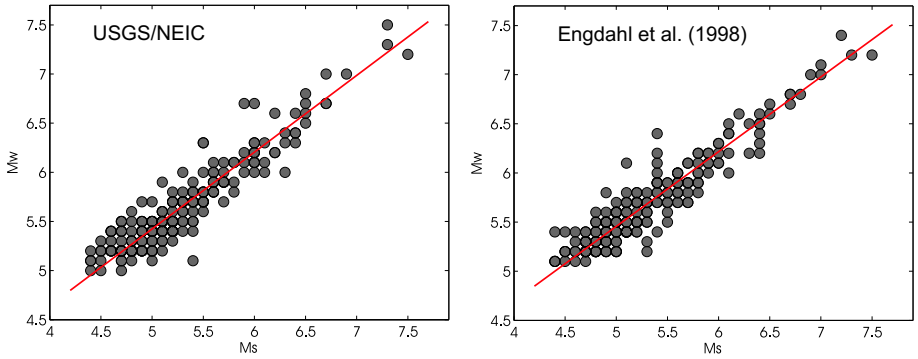

Fig. B.1: The surface-wave magnitude M_S is related to the moment magnitude M_w as shown in the above diagrams. The regressions were calculated according to the maximum likelihood approach assuming that the error for the two magnitude types is equal. Only those events were taken into consideration for which both magnitude types are available in the respective catalogue. On the left hand side, the calculation was performed for 225 events from the USGS/NEIC catalogue, on the right hand side for 529 events from the Engdahl catalogue. We obtained the following relations:
$M_w = 1.2690 M_S - 1.0436$ (USGS/NEIC) and
$M_w = 1.2765 M_S - 1.0825$ (Engdahl et al., 1998).

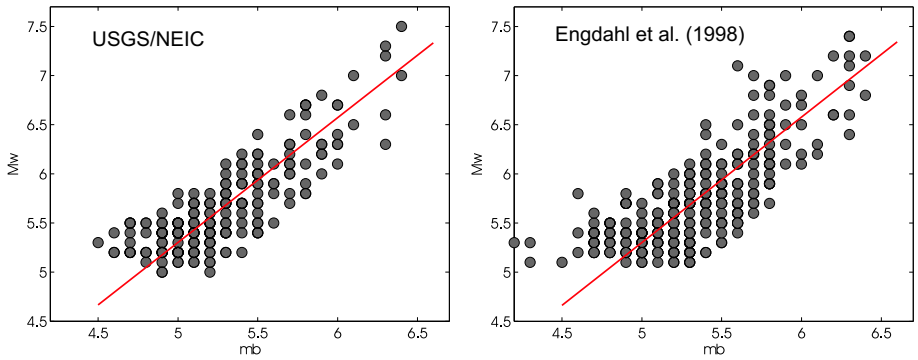

Fig. B.2: Analogous to Figure B.1 the regressions are based on the maximum likelihood approach. For the USGS/NEIC catalogue (left hand side) 371 events were considered, and for the Engdahl catalogue 866. Compared to the regressions derived above for the surface-wave magnitude (cf. Figure B.1), the data is more dispersed in this case. Nonetheless, the correspondence between the two regressions for the two different catalogues is satisfactory:
$M_w = 0.7813 m_b + 1.5175$ (USGS/NEIC) and
$M_w = 0.7601 m_b + 1.6562$ (Engdahl et al., 1998).

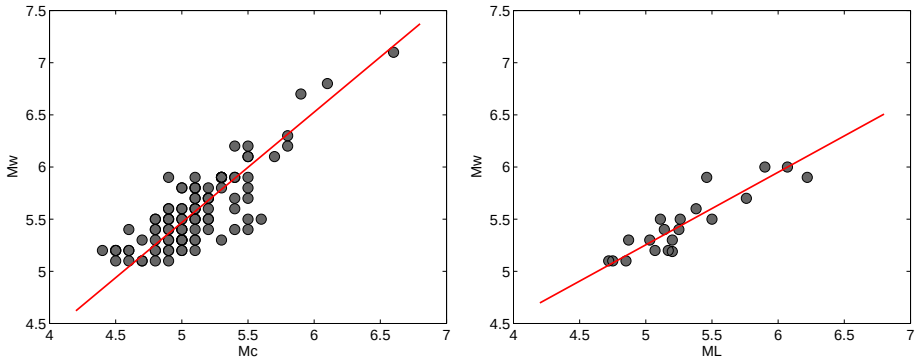

Fig. B.3: The local catalogues measure the size of the earthquakes in coda magnitude M_C (first measurement period) or in local magnitude M_L. In order to obtain corresponding M_w values for a local event, it was matched to the earthquakes listed by the USGS/NEIC catalogue. Two events are considered identical if they occurred less than 50km and less 20s apart from each other and differed by less than 1.5 units in magnitude (in order to rule out multiple matches between main- and foreshocks). The following regressions were obtained:
$M_w = 1.0583 M_C + 0.1765$ (left Figure) or
$M_w = 0.6960 M_L + 1.7738$ (right Figure).

C. Seismicity parameters for the detailed model

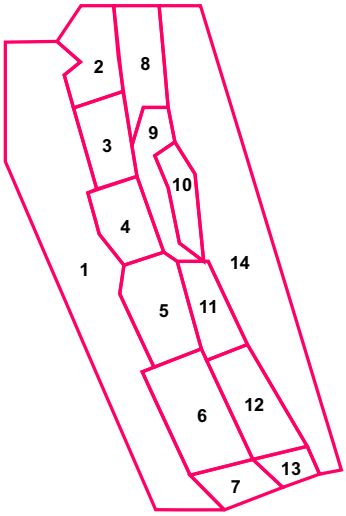

Nr.	Region	b-value	$\nu(4.5)$	Focal depths [km]	Maximum magnitudes
1	Diffuse (W)	1.58	3.26	10, 22, 34, 46, 58	6.55, 6.80, 7.05
2	North	0.71	7.49	20, 30, 40, 50, 60	8.05, 8.30, 8.55
3	Torres	0.71	6.21	12, 22, 32, 42, 58	7.75, 8.00, 8.25
4	Central	0.71	4.77	10, 22, 34, 46, 58	7.45, 7.70, 7.95
5	Efate	0.71	10.77	8, 18, 28, 38, 55	7.65, 7.90, 8.15
6	South	0.71	10.05	10, 25, 32, 40, 60	7.35, 7.60, 7.85
7	Loyalty	0.71	3.10	10, 25, 32, 40, 60	7.05, 7.30, 7.55
8	BA North	0.71	2.08	20, 30, 40, 50, 60	6.35, 6.60, 6.85
9	Aoba	0.71	3.59	10, 22, 34, 46, 58	7.75, 8.00, 8.25
10	CBAT	0.71	3.73	12, 20, 28, 35, 45	7.25, 7.50, 7.75
11	BA Efate	0.71	1.93	8, 15, 25, 40, 55	6.65, 6.90, 7.15
12	BA South	0.71	2.76	7, 20, 32, 40, 60	7.25, 7.50, 7.75
13	BA Loyalty	0.71	0.98	7, 20, 32, 40, 60	6.15, 6.40, 6.65
14	Diffuse (E)	1.58	3.03	10, 22, 34, 46, 58	6.25, 6.50, 6.75

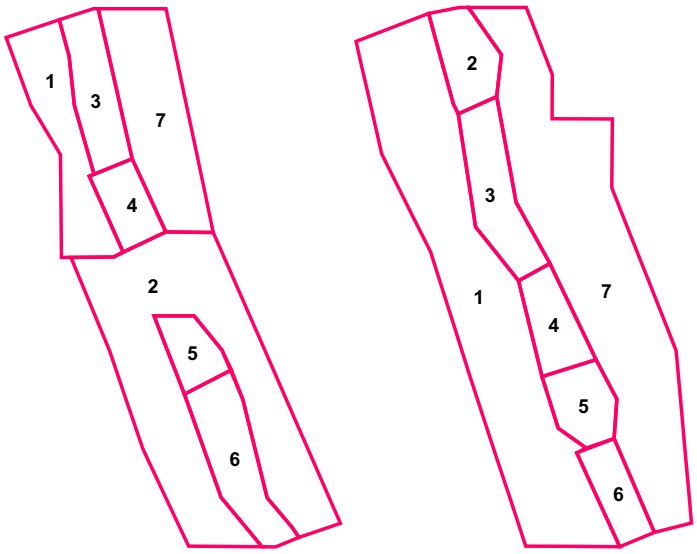

Referring to the left figure (depth range: $60 - 120$ km):

Nr.	Region	b-value	$\nu(4.5)$	Focal depths [km]	Maximum magnitudes
1	Diffuse (NW)	1.58	1.18	62, 75, 88, 101, 114	5.65, 5.90, 6.15
2	Diffuse (S)	1.58	1.57	62, 75, 88, 101, 114	5.65, 5.90, 6.15
3	North	0.65	8.97	65, 78, 85, 91, 115	7.65, 7.90, 8.15
4	Central	0.65	6.08	62, 69, 90, 111, 119	7.45, 7.70, 7.95
5	Gap	0.65	1.03	65, 70, 85, 105, 112	7.05, 7.30, 7.55
6	South	0.65	5.75	62, 75, 95, 109, 118	7.65, 7.90, 8.15
7	Diffuse (NE)	1.58	1.00	62, 75, 88, 101, 114	6.95, 7.20, 7.45

Referring to the right figure (depth range: $120 - 200$ km):

Nr.	Region	b-value	$\nu(4.5)$	Focal depths [km]	Maximum magnitudes
1	Diffuse (W)	1.58	1.18	135, 150, 165, 180, 195	5.65, 5.90, 6.15
2	North	0.75	4.36	135, 150, 165, 180, 195	7.05, 7.30, 7.55
3	Central	0.75	23.14	135, 150, 165, 180, 195	7.95, 8.20, 8.45
4	Gap	0.75	0.63	130, 140, 150, 175, 200	6.05, 6.30, 6.55
5	Tanna	0.75	4.33	135, 150, 165, 180, 195	7.95, 8.20, 8.45
6	South	0.75	2.61	130, 140, 150, 175, 200	7.55, 7.80, 8.05
7	Diffuse (E)	1.58	0.17	135, 150, 165, 180, 195	5.45, 5.70, 5.95

D. Acknowledgements

This report is the result of a joint cooperation between the GeoForschungsZentrum Potsdam (GFZ), Germany, the Institut de Recherche pour le Développement (IRD), France, and the South Pacific Applied Geoscience Commission (SOPAC), Fiji. SOPAC's long lasting experience and effort to assess natural hazards in the Pacific complemented the scientific investigations pursued and the local seismic data assembled by IRD. The GFZ contributed the scientific and technical expertise concerning probabilistic seismic hazard calculations and the financing during this final phase. The initial phase of the project was financed and supported by the Robert Bosch Foundation.

A long list of people apart from the authors have contributed to this study. We would like to thank those colleagues in Section 5.3 "Engineering Seismology" at the GeoForschungsZentrum Potsdam, who are not co-authors of this study, namely Dr. Dietrich Stromeyer, Dr. Rutger Wahlström, Uwe Lemgo, and Anna Wirth.

The "Communities at Risk"-Programm at the Secretariat of the South Pacific Applied Geoscience Commission (SOPAC) encouraged and enriched this study substantially. Specifically, we would like to thank Dr. Graham Shorten for his support and advice and Esline Garaebiti at the Department of Geology, Mines, and Water Resources, Vanuatu for her cooperation.

Last but not least we want to express our gratitude to Dr. Tono Eitel, Anke Schmidt (Robert Bosch Foundation) and Astrid Irrgang (Studienstiftung des deutschen Volkes) for their support and financing (in the context of the Postgraduate Programm for International Affairs) during the initial phase of this project.

Bibliography

Acharya, H.: 1971, Magnitude-frequency relations and deep-focus earthquakes, *Bull. Seis. Soc. Am.* **61**, 1345–1350.

Burne, R., Collot, J. and Daniel, J.: 1988, Superficial structures and stress regimes of the downgoing plate associated with subduction-collision in the central New Hebrides arc (Vanuatu), *in* H. Greene and F. Wong (eds), *Geology and Offshore Resources of Pacific Island Arcs, Vanuatu Region*, Vol. 8 of *Earth Science Series*, Circum Pacific Council for Energy and Mineral Resources, Houston, Texas, pp. 357–376.

Calmant, S., Pelletier, B., Lebellegard, P., Bevis, M., Taylor, F. and Phillips, D.: 2003, New insights on the tectonics along the New Hebrides subduction zone based on GPS results, *J. Geophys. Res.* **108**(B6), 2319.

Calmant, S., Pelletier, B., Pillet, R., Regnier, M., Lebellegard, P., Maillard, D., Taylor, F., Bevis, A. and Recy, J.: 1997, Interseismic and coseismic motions in GPS series related to the Mw 7.3 July 13, 1994, Malekula earthquake, central New Hebrides subduction zone, *Geophys. Res. Lett.* **24**(23), 3077–3080.

Charvis, P. and Pelletier, B.: 1989, The northern New Hebrides back-arc troughs: history and relation with the North Fiji Basin, *Tectonophysics* **170**, 259–277.

Chatelain, J. and Grasso, J.: 1992, Spatial and temporal seismic energy release in the Efate region (central New Hebrides island arc): Evidence for buckling?, *Geophys. Res. Lett.* **19**(11), 1157–1160.

Chatelain, J., Cardwell, B. I. R. and Prévot, R.: 1986, Patterns of seismicity associated with asperities in the central New Hebrides Island arc, *J. Geophys. Res.* **91**, 12497–12519.

Chatelain, J., Guillier, B. and Gratier, J.: 1993, Unfolding the subducting plate in the central New Hebrides Island Arc: Geometrical argument for detachment of part of the downgoing slab, *Geophys. Res. Lett.* **20**(8), 655–658.

Chatelain, J., Molnar, P., Prévot, R. and Isacks, B.: 1992, Detachment of part of the downgoing slab and uplift of the New Hebrides (Vanuatu) islands, *Geophys. Res. Lett.* **19**(14), 1507–1510.

Choudhury, M., Poupinet, G. and Perrier, G.: 1975, Shear velocity from differential travel times of short-period ScS-P in New Hebrides, Fiji-Tonga and Banda Sea regions, *Bull. Seism. Soc. Am.* **65**, 1787–1796.

Christova, C. and Scholz, C.: 2003, Stresses in the Vanuatu subducting slab: A test of two hypotheses, *Geophys. Res. Lett.*

Chung, W. and Kanamori, H.: 1978, A mechanical model for plate deformation associated with aseismic ridge subduction in the New Hebrides arc, *Tectonophysics* **50**, 29–40.

Colley, H. and Ash, R.: 1971, *The Geology of Erromango*, Reg.Rep. - New Hebrides Geological Survey.

Collot, J. and Fisher, M.: 1991, The collision zone between the north D'Entrecasteaux ridge and the New Hebrides island arc, 1, Sea beam morphology and shallow structure, *J. Geophys. Res.* **96**(B3), 4457–4478.

Collot, J., Daniel, J. and Burne, R.: 1985, Recent Tectonics associated with the subduction/collision of the D'Entrecasteaux Zone in the central New Hebrides, *Tectonophysics* **112**, 325–356.

Collot, J., Fisher, M. and Geist, E.: 1991a, The collision zone between the north D'Entrecasteaux ridge and the New Hebrides island arc, 2, Structure from multichannel seismic data, *J. Geophys. Res.* **96**(B3), 4479–4495.

Collot, J., Fisher, M. and Geist, E.: 1991b, Structure of the collision zone between Bougainville Guyot and the accretionary wedge of the New Hebrides island arc, southwest Pacific, *Tectonics* **10**(5), 887–903.

Cornell, C.: 1968, Engineering seismic risk analysis, *Bull. Seism. Soc. Am.* **58**, 1583–1606.

Crouse, C.: 1991, Ground-Motion Attenuation Equations for Earthquakes on the Cascadia Subduction Zone, *Earthq. Spectra* **7**(2), 201–236.

Daniel, J. and Katz, H.: 1981, D'Entrecasteaux Zone, trench and western chain of the central New Hebrides arc: their significance and tectonic relationship, *Geo-Mar. Lett.* **1**, 213–219.

Dupont, J.: 1979, Le système d'arc insulaire des Tonga et Kermadec: deux morphologies différentes, une seule zone de subduction (Pacifique Sud), *C.R. Acad. Sci. Paris* **D289**, 245–248.

Engdahl, E., van der Hilst, R. and Buland, R.: 1998, Global teleseismic earthquake relocation with improved travel times and procedures for depth determination, *Bull. Seism. Soc. Am.* **88**, 722–743.

Fisher, M., Greene, H., Geist, E. and Collot, J.: 1994, Seismic stratigraphy of the North Aoba Basin, central New Hebrides island arc, *in* C. O. Fox (ed.), *Proceedings of the Ocean Drilling Program, Scientific Results, 134*, Vol. 134, College Station, TX (Ocean Drilling Program), pp. 59–69.

Garaebiti, E., Shorten, G., Regnier, M., Naidu, P. and Swamy, M.: 2002, Assessment of the Port Vila Earthquake, Vanuatu, 2nd January 2002, *Technical Report JCO142*, DGMWR/IRD/SOPAC Joint Publication.

Gaull, B., Michael-Leiba, M. and Rynn, J.: 1990, Probabilistic earthquake risk maps of Australia, *Aust. J. Earth Sci.* **37**, 169–187.

Geist, E., Fisher, M. and Scholl, D.: 1993, Large scale deformation associated with subduction, *Geophys. J. Int.* **115**, 344–366.

Greene, H., Collot, J., Fisher, M. and Crawford, A.: 1994, Neogene tectonic evolution of the New Hebrides Island Arc: A review incorporating ODP Drilling results, *in* C. O. Fox (ed.), *Proceedings of the Ocean Drilling Program, Scientific Results, 134*, Vol. 134, College Station, TX (Ocean Drilling Program), pp. 19–46.

Grünthal, G.: 1985, The up-dated earthquake catalogue for the German Democratic Republic and adjacent areas - statistical data characteristics and conclusions for hazard assessment, *Proc. 3rd Int. Symp. on the Analysis of Seismicity and Seismic Risk*, Liblice Castle, Czechoslovakia.

Grünthal, G. and the GSHAP Region 3 Working Group: 1999, Seismic hazard assessment for central, north and northwest Europe: GSHAP Region 3, *Ann. Geofis.* **42**(6), 999–1011.

Grünthal, G., Bosse, C., Sellami, S., Mayer-Rosa, D. and Giardini, D.: 1999, Compilation of the GSHAP regional seismic hazard for Europe, Africa and the Middle East, *Ann. Geofis.* **42**(6), 1215–1223.

Gutenberg, B. and Richter, C.: 1944, Frequency of earthquakes in California, *Bull. Seism. Soc. Am.* **34**, 185–188.

Habermann, R.: 1984, Spatial seismicity variations and asperities in the New Hebrides seismic zone, *J. Geophys. Res.* **89**, 5891–5903.

Hamburger, M. and Isacks, B.: 1988, Diffuse back-arc deformation in the southwestern Pacific, *Nature* **332**, 599–604.

Hofstetter, A., Shapira, A., Bulehite, K., Jones, T., Mafi, K., Malitzky, A., Papabatu, A., Prasad, G., Regnier, M., Shorten, G., Singh, A., Stephen, M. and Vuetibau, L.: 2000, Frequency-Magnitude Relationships for seismic areas around the capital cities of Solomon, Vanuatu, Tonga and Fiji Islands, *J. of Seismolog.* **4**, 285–296.

Jones, T.: 1997, Probabilistic Earthquake Hazard Assessment for Fiji, *Technical Report 46*, AGSO Record, Canberra.

Lagabrielle, Y., Pelletier, B., Cabioch, G., Regnier, M. and Calmant, S.: 2003, Coseismic and long-term vertical displacement due to back arc shortening, Central Vanuatu: Offshore and onshore data following the Ms 7.5, 26 November 1999, Ambrym earthquake, *J. Geophys. Res.*

Louat, R. and Pelletier, B.: 1989, Seismotectonics and present day relative plate motions in the New Hebrides-North Fiji Basin region, *Tectonophysics* **167**, 41–55.

Lussou, P., Bard, P. and Cotton, F.: 2001, Seismic Design Regulation Codes: Contribution of K-net data to site effect evaluation, *J. Earthq. Eng.* **5**(1), 13–33.

Maillet, P., Monzier, M., Selo, M. and Storzer, D.: 1983, The D'Entrecasteaux Zone (South-West Pacific) - a petrological and geochronological reappraisal, *Mar. Geol.* **53**, 179–198.

McCue, K.: 1999, Seismic hazard mapping in Australia, the Southwest Pacific and Southeast Asia, *Ann. Geofis.* **42**(6), 1191–1198.

McGuire, R.: 1976, Fortran computer program fo seismic risk analysis, *Technical Report 76-77*, US Geological Survey Open File Report.

Meffre, S. and Crawford, A.: 2001, Collision tectonics in the New Hebrides arc (Vanuatu), *The Island Arc* **10**, 33–50.

Mellors, R., Chatelain, J., Isacks, B., Hade, G., Bevis, M. and Prévot, R.: 1991, A tilt and seismicity episode in the New Hebrides (Vanuatu) island arc, *J. Geophys. Res.* **96**(B10), 16,535–16,546.

Musson, R.: 1999, Probabilistic seismic hazard maps for the North Balkan region, *A. di Geofis.* **6**, 1109–1138.

Parolai, S., Grünthal, G. and Wahlström, R.: 2005 (submitted), Site specific response spectra from the combination of microzonation with probabilistic seismic hazard assessment - an example for the Cologne (Germany) area, *Soil Dyn. Earthq. Eng.*

Pascal, G.: 1974, *Contribution à l'étude de la sismicité des Nouvelles-Hebrides.*, PhD thesis, Faculté des Sciences de l'Université de Paris VI.

Pelletier, B., Calmant, S. and Pillet, R.: 1998, Current tectonics of the Tonga-New Hebrides region, *Earthq. Plan. Sci. Lett.* **164**, 263–276.

Pelletier, B., Meschede, M., Chabernaud, T., Roperch, P. and Zhao, X.: 1994, Tectonics of the central New Hebrides Arc, North Aoba Basin, *in* C. O. Fox (ed.), *Proceedings of the Ocean Drilling Program, Scientific Results, 134*, Vol. 134, College Station, TX (Ocean Drilling Program), pp. 19–46.

Pontoise, B. and Tiffin, D.: 1986, Seismic refraction results over d'Entrecasteaux Zone west of the New Hebrides arc, *Géodynamique* **1**, 109–120.

Prévot, R. and Chatelain, J.: 1984, Sismicité et risque sismique à Vanuatu, *Technical report*, ORSTOM.

Prévot, R., Chatelain, J., Roecker, S. and Grasso, J.: 1994, A shallow double seismic zone beneath the central New Hebrides (Vanuatu): Evidence for fragmentation and accretion of the descending plate?, *Geophys. Res. Lett.* **21**(19), 2159–2162.

Prévot, R., Roecker, S., Isacks, B. and Chatelain, J.: 1991, Mapping of low P wave velocity structures in the subducting plate of the central New Hebrides, southwest Pacific, *J. Geophys. Res.* **96**(B12), 19,825–19,842.

Reasenberg, P.: 1985, Second-order moment of central California seismicity, *J. Geophys. Res.* **90**, 5479–5496.

Regnier, M., Moris, S., A.Shapira, Malitzky, A. and Shorten, G.: 2000, Microzonation of the expected seismic site effects across Port Vila, Vanuatu, *J. of Earthq. Eng.* **4**(2), 215–231.

Risk Engineering Ltd.: 1997, *FRISK88M© User's Manual, up-dated version 1.70.*

Roecker, S., Chatelain, J., Isacks, B. and Prévot, R.: 1988, Anomalously deep earthquakes beneath the New Hebrides Trench, *Bull. Seism. Soc. Am.* **78**, 1984–2007.

Shedlock, K., Giardini, D., Grünthal, G. and Zhang, P.: 2000, The GSHAP Global Seismic Hazard Map, *Seism. Res. Lett.* **71**(6), 679–689.

Smalley, R., Chatelain, J., Turcotte, D. and Prévot, R.: 1987, A fractal approach to the clustering of earthquakes: applications to the seismicity of the New Hebrides, *Bull Seism. Soc. Am.* **77**, 1368–1381.

Stirling, W., McVerry, G. and Berryman, K.: 2002, A New Seismic Hazard Model for New Zealand, *Bull. Seism. Soc. Am.* **92**(5), 1878–1903.

Takahashi, T., Kobayashi, S., Fukushima, Y., Zhao, J., Nakamura, H. and Somerville, P.: 2000, A spectral Attenuation Model for Japan using strong motion data base, *Proceedings of the Sixth International Conference on Seismic Zonation*.

Taylor, F., Bevis, M. and Schutz, B.: 1995, Geodetic measurements of convergence at the New Hebrides island arc indicate arc fragmentation caused by an impinging aseismic ridge, *Geology* **23**, 1011–1014.

Taylor, F., Edwards, R., Wasserburg, G. and Frohlich, C.: 1990, Seismic recurrence intervals and timing of aseismic subduction inferred from emerged corals and reefs of the Central Vanuatu (New Hebrides) frontal arc, *J. Geophys. Res.* **95**(B1), 393–408.

Vogt, P., Lowrie, A., Bracey, D. and Hey, R.: 1976, Subduction of aseismic oceanic ridges: effects on shape, seismicity, and other characteristics of consuming plate boundaries, *Geol. Soc. Am., Spec. Pap.* **172**, 59.

Wyss, M. and Toya, Y.: 2000, Is Background Seismicity Produced at a Stationary Poissonian Rate?, *Bull. Seism. Soc. Am.* **90**(5), 1174–1187.

Wyss, M., Habermann, R. and Heiniger, C.: 1983, Seismic quiescence stress drops and asperities in the New Hebrides Arc, *Bull. Seism. Soc. Am.* **73**, 219–236.

Youngs, R., Chiou, S., Silva, W. and Humphrey, J.: 1997, Strong Ground Motion Attenuation Relationships for Subduction Zone Earthquakes, *Seism. Res. Let.* **68**(1), 58–73.